Inorganic Chemistry

Article

pubs.acs.org/IC

What a Difference a Carbon Makes: H_4octapa vs H_4C3octapa, Ligands for In-111 and Lu-177 Radiochemistry

Eric W. Price,[†,‡] Brian M. Zeglis,[§] Jacqueline F. Cawthray,[†,‡] Jason S. Lewis,*[,§] Michael J. Adam,*[,‡] and Chris Orvig*[,†]

[†]Medicinal Inorganic Chemistry Group, Department of Chemistry, University of British Columbia, 2036 Main Mall, Vancouver, British Columbia V6T 1Z1, Canada

[‡]TRIUMF, 4004 Wesbrook Mall, Vancouver, British Columbia V6T 2A3, Canada

[§]Department of Radiology and Program in Molecular Pharmacology and Chemistry, Memorial Sloan Kettering Cancer Center, 1275 York Avenue, New York, New York 10065, United States

Supporting Information

ABSTRACT: The acyclic ligands H_4C3octapa and *p*-SCN-Bn-H_4C3octapa were synthesized for the first time, using nosyl protection chemistry. These new ligands were compared to the previously studied ligands H_4octapa and *p*-SCN-Bn-H_4octapa to determine the extent to which the addition of a single carbon atom to the backbone of the ligand would affect metal coordination, complex stability, and, ultimately, utility for in vivo radiopharmaceutical applications. Although only a single carbon atom was added to H_4C3octapa and the metal donor atoms and denticity were not changed, the solution chemistry and radiochemistry properties were drastically altered, highlighting the importance of careful ligand design and radiometal−ligand matching. It was found that $[In(C3octapa)]^-$ and $[Lu(C3octapa)]^-$ were substantially different from the analogous H_4octapa complexes, exhibiting fluxional isomerization and a higher number of isomers, as observed by ^{1}H NMR, VT-NMR, and 2D COSY/HSQC-NMR experiments. Past evaluation of the DFT structures of $[In(octapa)]^-$ and $[Lu(octapa)]^-$ revealed very symmetric complexes; in contrast, the $[In(C3octapa)]^-$ and $[Lu(C3octapa)]^-$ complexes were much less symmetric, suggesting lower symmetry and less rigidity than that of the analogous H_4octapa complexes. Potentiometric titrations revealed the formation constants (log K_{ML}, pM) were ∼2 units lower for the In^{3+} and Lu^{3+} complexes of H_4C3octapa when compared to that of the more favorable H_4octapa ligand (∼2 orders of magnitude less thermodynamically stable). The bifunctional ligands *p*-SCN-Bn-H_4C3octapa and *p*-SCN-Bn-H_4octapa were conjugated to the antibody trastuzumab and radiolabeled with ^{111}In and ^{177}Lu. Over a 5 day stability challenge experiment in blood serum, ^{111}In-octapa− and ^{111}In-C3octapa−trastuzumab immunoconjugates were determined to be ∼91 and ∼24% stable, respectively, and ^{177}Lu-octapa− and ^{177}Lu-C3octapa−trastuzumab, ∼89% and ∼4% stable, respectively. This work suggests that 5-membered chelate rings are superior to 6-membered chelate rings for large metal ions like In^{3+} and Lu^{3+}, which is a crucial consideration for the design of bifunctional chelates for bioconjugation to targeting vectors for in vivo work.

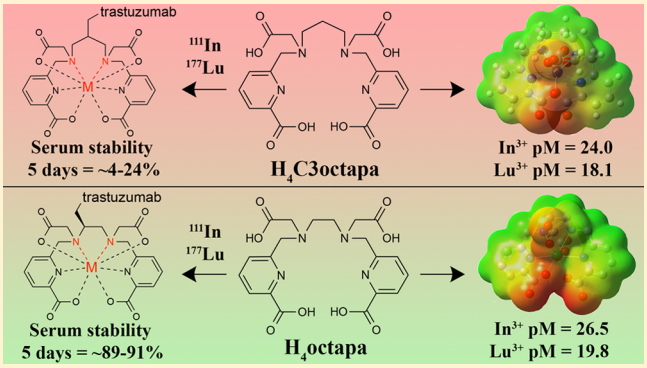

INTRODUCTION

In recent years, radiometal-based radiopharmaceuticals have become increasingly appreciated for their potential in diagnostic and therapeutic medicine.[1−10] The modular and versatile nature of these systems allows for a continually increasing number of routinely produced radiometals to be harnessed for single photon emission computed tomography (SPECT), positron emission tomography (PET), and therapy (e.g., Auger electron, β^-, α).[1−10] Radiometal-based radiopharmaceuticals are typically broken down into several modules and can be assembled in many permutations for a high degree of customization: the targeting vector (e.g., peptide, antibody, nanoparticle) is selected for site-specific delivery to a chosen biological target or compartment; the bifunctional chelator (BFC) is selected for optimal stability and radiolabeling properties with the chosen radiometal; the bioconjugation method is selected based on the reactivity and functional groups available on the bifunctional chelator and targeting vector; and, finally, the radiometal is selected for its decay characteristics.[1−9] Even subtle changes to the ligand structure, site of conjugation, and donor arms of ligands can cause drastic changes to their radiolabeling properties and the stability of their radiometal complexes. These ligand alterations can include the addition of functional groups to allow for conjugation with targeting vectors (e.g., *p*-benzyl-isothiocya-

Received: June 23, 2014
Published: September 5, 2014

   dx.doi.org/10.1021/ic501466z | Inorg. Chem. 2014, 53, 10412−10431

Chart 1. Structures of Selected Chelators[a]

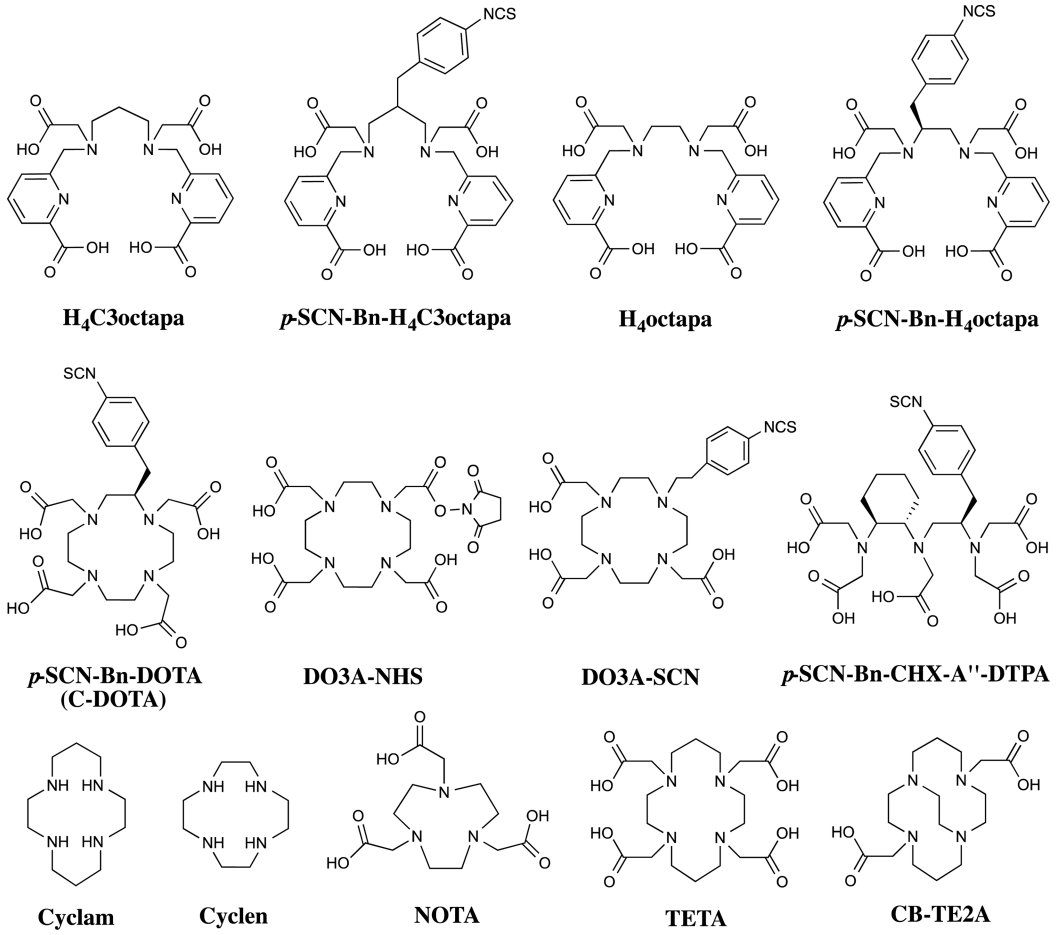

[a]Two pyridinecarboxylate-based ligands that differ by only 1 carbon, H_4C3octapa (propylene-bridged) and H_4octapa (ethylene-bridged); their bifunctional derivatives *p*-SCN-Bn-H_4C3octapa and *p*-SCN-Bn-H_4octapa; the popular ^{111}In/^{177}Lu/$^{86/90}$Y bifunctional ligands C-DOTA, DO3A-NHS, DO3A-SCN, and *p*-SCN-Bn-CHX-A″-DTPA; and other ligand examples Cyclam, Cyclen, NOTA, TETA, and CB-TE2A.

nate, maleimide, activated esters), changes to ligand donor arms and ligand denticity (e.g., peptide coupling to a carboxylate donor arm), and changing ligand donor types (e.g., changing primary amines to secondary amines, or methylenephosphonates for carboxylates), and the effects of these changes on radiolabeling and stability properties can be significant.[1−10] The difference in stability and radiolabeling kinetics between acyclic and macrocyclic ligands is often significant, as macrocycles provide a degree of preorganization of the metal binding cavity, which provides a strong entropic incentive for metal complexation, although typically at the cost of slow reaction kinetics.[11−13] There are a number of competent and well-studied bifunctional chelators available for use; however, none are without shortcomings, and for purposes ranging from enhancing radiolabeling kinetics to enhancing kinetic inertness and in vivo stability, development of new bifunctional chelators is an important field of study.[3,7,8,14,15]

The literature is rich with examples of how small changes in cavity size, chelate-ring size, bifunctionalization site, and coordination environment can make drastic changes in the stability of radiometal complexes. This article discusses differences in binding of two structurally similar acyclic ligands to the specific radiometals ^{111}In and ^{177}Lu. Although each radiometal ion has unique aqueous chemistry properties, and the difference between macrocyclic and acyclic ligands is substantial, examples using different metal ions and both acyclic and macrocyclic ligands will be discussed. As an example of cavity size effects, the chemistry of the positron-emitting radiometal ion $^{64}Cu^{2+}$ with the widely used, macrocyclic chelators DOTA and NOTA provides an excellent illustration of the importance of the careful consideration of ligand properties (Chart 1). The denticity and cavity size of the macrocycle NOTA is smaller than that of DOTA (6 vs 8 maximum denticity) and therefore is a better fit for radiometals such as ^{64}Cu and ^{68}Ga, resulting in increased stability and inertness of these metal complex.[16−21] A common site of bifunctional derivatization of DOTA is one of its 4 carboxylic acid arms, which effectively masks one of the carboxylic acid chelating arms, effectively dropping the denticity from 8 to 7 (although the carbonyl can still coordinate to metal ions, albeit weakly).[22] This is a good example of how changing ligand donor groups can effect the stability of radiometal complexes, as this functionalization of DOTA causes a noted decrease in the in vitro and in vivo stability of its radiometal complexes with isotopes like ^{111}In (DO3A, Chart 1).[22] An example of how ligand isomers can affect stability is the acyclic ligand CHX-DTPA, where 4 possible ligand isomers can be synthesized, with CHX-A″-DTPA being the most stable isomer by a substantial margin (Chart 1).[23,24] Another example of how subtle changes in ligand donor groups can effect stability are

dx.doi.org/10.1021/ic501466z | Inorg. Chem. 2014, 53, 10412−10431

macrocyclic TE2A derivatives (cyclam-based, Chart 1), which undergo remarkable changes in radiolabeling and stability properties as a result of simply alkylating the two secondary amine groups of TE2A to form tertiary amines, either with methyl groups (MM/DM-TE2A) or an ethylene bridge (CB-TE2A).[25,26] The result of these TE2A modifications are that a large improvement in the in vitro and in vivo stability of the ^{64}Cu complexes of MM/DM-TE2A is observed, relative to that of TE2A.[25,26]

An example of the predilection certain radiometals have for 5- or 6-membered chelate rings can be found when comparing the stability of cyclam- and cyclen-based ligands with the Cu^{2+} isotope ^{64}Cu.[25,27] The inclusion of some 6-membered chelate rings (cyclam-based) in ligands such as TETA and CB-TE2A yields some improvements in stability in vitro and in vivo when compared to that for ligands that contain only 5-membered chelate rings (cyclen-based) such as DOTA and CB-DO2A.[25] These findings suggest that 6-membered chelate rings may work well with Cu^{2+}, at least when comparing the specific ligand scaffolds of cyclen and cyclam.[27] In this specific example, it appears that copper prefers some 6-membered chelate rings (TETA) to strictly 5-membered chelate rings (DOTA); however, the smaller macrocycle NOTA forms more stable complexes with Cu^{2+} than TETA while forming only 5-membered chelate rings.[16,17] Conversely, previous work in our laboratory on the chelation of Ga^{3+} with the ligand H_2dedpa suggested a better fit for Ga^{3+}, which is even smaller than Cu^{2+} (62 vs 73 pm for CN = 6, respectively), with 5-membered chelate rings over 6-membered chelate rings.[15] The discussion of which chelate ring-size is the best fit and the most stable for large metal ions such as In^{3+}, Lu^{3+}, and Y^{3+} is less opaque. DOTA has been shown to be superior to TETA for large metal ions like In^{3+}, Lu^{3+}, and Y^{3+}, suggesting that the optimal stability of large metal ions is achieved when using 5-membered chelate rings, which supports this work comparing H_4octapa to H_4C3octapa.[2,3,7,8] These examples demonstrate the lack of clarity for the preference of some metal ions between 5- and 6-membered chelate rings, providing a compelling reason to perform further studies on the subject.

We have previously published work on the acyclic ligand H_4octapa and the bifunctional derivative *p*-SCN-Bn-H_4octapa, which showed very promising ambient temperature radiolabeling performance and in vitro and in vivo stability with ^{111}In and ^{177}Lu. This study was performed by conjugating *p*-SCN-Bn-H_4octapa to an antibody (trastuzumab) as a proof-of-principle targeting vector for HER2/*neu*-expressing ovarian cancer cells (SKOV3).[14,28] Largely due to their exceptional specificity and affinity, antibodies are extremely useful targeting vectors for the delivery of radioactive isotopes to cancerous tissues.[29,13] Antibodies also possess long biological half-lives (~2 to 3 weeks in vivo), which makes them excellent vehicles for proof-of-principle studies of new bifunctional ligands in which stability in vitro and in vivo must be studied for several days/weeks.[13] The isotopes ^{111}In and ^{177}Lu are widely used in both research and clinical settings, with ^{111}In being a cyclotron-produced radiometal (^{111}Cd(p,n)^{111}In) for SPECT imaging ($t_{1/2}$ ~ 2.8 days) and Auger electron therapy and ^{177}Lu being a reactor-produced therapeutic radiometal (^{176}Lu(n,γ)^{177}Lu) that emits β^- particles as well as γ-rays ($t_{1/2}$ ~ 6.6 days).[30]

To further evaluate the impact of ligand structure changes on radiolabeling efficiency and stability, we have synthesized the novel derivative of H_4octapa, H_4C3octapa, modified with only a single additional carbon atom (1,3-propylenediamine vs 1,2-ethylenediamine backbone) (Chart 1). Herein, we report the synthesis, characterization, In^{3+}/Lu^{3+} metal complexation, density functional theory (DFT) structure prediction, potentiometric titrations to determine thermodynamic stability constants, and ^{111}In/^{177}Lu radiolabeling and in vitro blood serum stability of the new ligand H_4C3octapa and its bifunctional derivative *p*-SCN-Bn-H_4C3octapa (Chart 1). In this study, we have conjugated both the new *p*-SCN-Bn-H_4C3octapa and the previously studied *p*-SCN-Bn-H_4octapa to the HER2/*neu*-targeted antibody trastuzumab and directly compared their properties. The purpose of this work was to determine the extent to which a small structural change of the ligand, which, importantly, does not change the ligand denticity or metal coordinating groups, may affect radiolabeling performance and most importantly the stability of radiometal complexes. Our laboratory has been studying new acyclic chelators based on the pyridinecarboxylate scaffold for several years now, and this work aims to expand upon our understanding of ligand design and radiometal−ligand matching (Chart 1).[14,15,31−37]

EXPERIMENTAL SECTION

Materials and Methods. All solvents and reagents were purchased from commercial suppliers (Sigma-Aldrich, St. Louis, MO; TCI America, Portland, OR; Fisher Scientific, Waltham, MA) and were used as received unless otherwise indicated. The bifunctional chelator *p*-SCN-Bn-H_4octapa was synthesized as previously described.[28] DMSO used for chelator stock solutions was of molecular biology grade (>99.9%: Sigma, D8418). 1,4,7,10-Tetraazacyclododecane-1,4,7,10-tetraacetic acid *para*-benzylisothiocyanate (*p*-SCN-Bn-DOTA) was purchased from Macrocyclics, Inc. (Dallas, TX). Methyl-6-bromomethylpicolinate was synthesized according to a literature protocol.[14] Water used was ultrapure (18.2 MΩ cm^{-1} at 25 °C, Milli-Q, Millipore, Billerica, MA). The analytical thin-layer chromatography (TLC) plates were aluminum-backed ultrapure silica gel (Siliaplate, 60 Å pore size, 250 μM plate thickness, Silicycle, Quebec, QC). Flash column silica gel was provided by Silicycle (Siliaflash Irregular Silica Gels F60, 60 Å pore size, 40−63 mm particle size, Silicycle, Quebec, QC). Automated column chromatography was performed using a Teledyne Isco (Lincoln, NE) CombiFlash R_f automated system with solid load cartridges packed with flash column silica gel and RediSep R_f Gold reusable normal-phase silica columns and neutral alumina columns (Teledyne Isco, Lincoln, NE). ^{1}H and ^{13}C NMR spectra were recorded on Bruker AV300, AV400, or AV600 instruments; all spectra were internally referenced to residual solvent peaks except for ^{13}C NMR spectra in D_2O, which were externally referenced to a sample of CH_3OH/D_2O. Low-resolution mass spectrometry was performed using a Waters liquid chromatography−mass spectrometer (LC−MS) consisting of a Waters ZQ quadrupole spectrometer equipped with an ESCI electrospray/chemical ionization ion source and a Waters 2695 HPLC system (Waters, Milford, MA). High-resolution electrospray−ionization mass spectrometry (ESI−MS) was performed on a Waters Micromass LCT time-of-flight instrument. Microanalyses for C, H, and N were performed on a Carlo Erba EA 1108 elemental analyzer. The HPLC system used for purification of nonradioactive compounds consisted of a semipreparative reverse-phase C18 Phenomenex synergi hydro-RP (80 Å pore size, 250 × 21.2 mm, Phenomenex, Torrance, CA) column connected to a Waters 600 controller, a Waters 2487 dual-wavelength absorbance detector, and a Waters delta 600 pump. ^{177}Lu(chelate) analysis was performed using an HPLC system comprised of a Shimadzu SPD-20A prominence UV/vis, LC-20AB prominence LC, a Bioscan flow-count radiation detector, and a C_{18} reverse-phase column (Phenomenex Luna Analytical 250 × 4.6 mm). UV/vis measurements for determining antibody stock solution concentrations were taken on a Thermo Scientific Nanodrop 2000 spectrophotometer (Wilmington, DE).

^{111}In was cyclotron produced (Advanced Cyclotron Systems, Model TR30) by proton bombardment through the reactions ^{111}Cd(p,n)^{111}In and was provided by Nordion as $^{111}InCl_3$ in 0.05 M HCl. ^{177}Lu was procured from PerkinElmer (PerkinElmer Life and Analytical Sciences, Wellesley, MA, effective specific activity of 29.27 Ci/mg) as $^{177}LuCl_3$ in 0.05 M HCl. Labeling reactions were monitored using silica-gel impregnated glass-microfiber instant thin-layer chromatography paper (iTLC-SG, Varian, Lake Forest, CA) and analyzed on a Bioscan AR-2000 radio-TLC plate reader using Winscan Radio-TLC software (Bioscan Inc., Washington, DC). All radiolabeling chemistry was performed with ultrapure water (>18.2 MΩ cm^{-1} at 25 °C, Milli-Q, Millipore, Billerica, MA) that had been passed through a 10 cm column of Chelex resin (BioRad Laboratories, Hercules, CA). Human blood serum (Sigma, Sera, human, aseptically filled, S7023-100mL) competition solutions were agitated at 550 rpm and held at 37 °C using an Eppendorf thermomixer, and then ^{177}Lu(chelate) mixtures were analyzed using GE Healthcare Life Sciences PD-10 desalting columns (GE Healthcare, United Kingdom, MW < 5000 Da filter) that were conditioned by elution of 25 mL phosphate-buffered saline (PBS) before use. ^{177}Lu/^{111}In-immunoconugates were analyzed using iTLC as described above and purified using PD-10 desalting columns and Corning 50k MW Amicon Ultra centrifugation filters. Radioactivity in samples was measured using a Capintec CRC-15R dose calibrator (Capintec, Ramsey, NJ).

***N,N′*-(2-Nitrobenzenesulfonamide)-1,3-diaminopropane (1).** Propylenediamine (173 μL, 2.05 mmol) was dissolved in THF (10 mL) and placed in an ice bath; then, sodium bicarbonate (~1 g) was added, followed by slow addition of 2-nitrobenzenesulfonyl chloride (0.954 g, 4.31 mmol). The reaction mixture was allowed to warm to ambient temperature and stirred overnight. The yellow mixture was filtered to remove sodium bicarbonate, rotary evaporated to a red oil, purified by silica chromatography (CombiFlash R_f automated column system; 120 g HP silica; A: dichloromethane, isocratic elution), and dried in vacuo to yield the product (**1**) as yellow solid (75%, ~0.684 g). ^{1}H NMR (300 MHz, $CDCl_3$, 25 °C) δ 8.13−8.06 (m, 2H), 7.97−7.84 (m, 6H), 6.65 (br s, 2H, -NH-), 3.19 (m, 4H), 1.81 (quin, J = 6.9 Hz, 2H). ^{13}C NMR (75 MHz, DMSO-d_6, 25 °C) δ 149.5, 135.2, 134.6, 133.9, 131.7, 126.2, 41.9, 31.2. HR-ESI-MS calcd for $[C_{15}H_{16}N_4O_8S_2+H]^+$, 445.0488; found, 445.0481 $[M + H]^+$, PPM = −1.5.

***N,N′*-(2-Nitrobenzenesulfonamide)-*N,N′*-[6-(methoxycarbonyl)pyridin-2-yl]methyl]-1,3-diaminopropane (2).** To a solution of **1** (0.418 g, 0.941 mmol) in dimethylformamide (10 mL, dried over molecular sieves 4 Å) were added methyl-6-bromomethyl picolinate[14] (0.476 g, 2.07 mmol) and sodium carbonate (~1 g). The faint yellow reaction mixture was stirred at 50 °C overnight, filtered to remove sodium carbonate, and concentrated in vacuo. The crude product was purified by silica chromatography (CombiFlash R_f automated column system; 80 g HP silica; A: chloroform, B: methanol, 100% A to 25% B gradient) to yield the product **2** as yellow solid (98%, ~0.685 g). ^{1}H NMR (300 MHz, $CDCl_3$, 25 °C) δ 8.03−7.93 (m, 4H), 7.78−7.73 (m, 2H), 7.68−7.52 (m, 8H), 4.60 (s, 4H), 3.93 (s, 6H), 3.25 (t, J = 7.0 Hz, 4H), 1.64−1.57 (m, 2H). ^{13}C NMR (75 MHz, $CDCl_3$, 25 °C) δ 165.1, 156.6, 147.8, 147.3, 137.9, 133.7, 132.5, 131.9, 130.7, 125.4, 124.1, 124.0, 52.8, 52.7, 45.9, 26.3. HR-ESI-MS calcd for $[C_{31}H_{30}N_6O_{12}S_2+H]^+$, 743.1441; found, 743.1440, $[M + H]^+$, PPM = −0.1.

***N,N′*-[6-(Methoxycarbonyl)pyridin-2-yl]methyl-1,3-diaminopropane (3).** To a solution of **2** (0.685 g, 0.922 mmol) in tetrahydrofuran (10 mL) was added thiophenol (223 μL, 2.03 mmol) and potassium carbonate (excess, ~0.4 g). The reaction mixture was stirred at 60 °C for 48 h, during which time the color changed from light yellow to dark yellow. The reaction mixture was filtered with a large fritted glass filter to remove K_2CO_3, rinsed liberally with THF and CH_3CN, and then concentrated to dryness in vacuo. The resulting crude yellow oil was purified by alumina chromatography (CombiFlash R_f automated column system; 24 g neutral alumina; A: dichloromethane, B: methanol, 100% A to 30% B gradient) to yield **3** as yellow oil (89%, ~0.306 g). Compound **3** was purified using neutral alumina, as it demonstrates an abnormally high affinity for silica and requires the use of ammonium hydroxide and >20% methanol to be eluted, resulting in partial methyl-ester deprotection and dissolving of some silica. ^{1}H NMR (300 MHz, $CDCl_3$, 25 °C) δ 7.95−7.93 (m, 2H), 7.77−7.74 (m, 2H), 7.54−7.52 (m, 2H), 4.01 (s, 4H), 3.92 (s, 6H), 3.61 (br s, -NH-, 2H), 2.81 (s, 4H), 1.78 (s, 2H). ^{13}C NMR (75 MHz, $CDCl_3$, 25 °C) δ 165.5, 159.5, 147.3, 137.4, 125.7, 123.5, 54.3, 52.7, 48.0, 28.6. HR-ESI-MS calcd for $[C_{19}H_{24}N_4O_4+H]^+$, 373.1876; found, 373.1881, $[M + H]^+$, PPM = 1.3.

***N,N′*-[(*tert*-Butoxycarbonyl)methyl-*N,N′*-[6-(methoxycarbonyl)pyridin-2-yl]methyl]-1,3-diaminopropane (4).** To a solution of **3** (188.3 mg, 0.506 mmol) in acetonitrile (10 mL) was added *tert*-butylbromoacetate (172 μL, 1.16 mmol) and sodium carbonate (~200 mg). The reaction mixture was stirred at 60 °C overnight. Sodium carbonate was removed by filtration, and the crude reaction mixture was concentrated in vacuo. The crude oil was purified by column chromatography (CombiFlash R_f automated column system; 40 g HP silica; A: dichloromethane, B: methanol, 100% A to 20% B gradient) to afford the product **4** as yellow oil (91%, ~0.276 g). ^{1}H NMR (300 MHz, $CDCl_3$, 25 °C) δ 7.94−7.91 (m, 2H), 7.72−7.71 (m, 4H), 3.94 (s, 6H), 3.92 (s, 4H), 3.20 (s, 4H), 2.64−2.60 (m, 4H), 1.62−1.58 (m, 2H), 1.39 (s, 18H). ^{13}C NMR (75 MHz, $CDCl_3$, 25 °C) δ 170.3, 165.8, 160.8, 147.1, 137.3, 126.0, 123.5, 80.9, 60.5, 56.3, 52.7, 52.4, 28.0. HR-ESI-MS calcd for $[C_{31}H_{44}N_4O_8+H]^+$, 601.3237; found, 601.3244, $[M + H]^+$, PPM = 1.2.

H_4C3octapa, *N,N′*-(6-Carboxy-2-pyridylmethyl)-*N,N′*-diacetic Acid-1,3-diaminopropane (5). To a solution of **4** (248 mg, 0.413 mmol) in a mixture of tetrahydrofuran/deionized water (3:1, 5 mL) was added LiOH (150 mg). The reaction mixture was stirred at ambient temperature for 4 h. A portion of HCl was added (5 mL, 6 M), and then the mixture was reduced to dryness in vacuo. The mixture was dissolved in deionized water (4 mL) and purified via semipreparative reverse-phase HPLC (10 mL/min, gradient: A: 0.1% TFA (trifluoroacetic acid) in deionized water, B: CH_3CN. 5 to 100% B linear gradient in 30 min. t_R = 11.5−13.3 min, broad). Product fractions were pooled, concentrated in vacuo, dissolved in HCl (5 mL, 6 M), and then concentrated in vacuo again to remove trifluoroacetic acid. This processes was repeated three times to remove traces of TFA. The HCl salt H_4C3octapa·4HCl·2H_2O (**5**) was obtained as a yellow solid (74% yield, ~0.195 g, using the molecular weight of the HCl salt as determined by elemental analysis). ^{1}H NMR (600 MHz, D_2O) δ 7.79 (br s, 4H, pyr-*H*), 7.43 (br s, 2H, pyr-*H*), 4.56 (s, 4H, Pyr-CH_2-N), 4.09 (s, 4H, HOOC-CH_2-N), 3.30 (br s, 4H, propylene-1,3-*H*), 1.95 (m, 2H, propylene-2-*H*). ^{13}C NMR (150 MHz, D_2O) δ 167.2, 166.1, 148.9, 145.2, 139.5, 126.7, 126.5, 125.1, 57.4, 54.6, 52.7, 19.4. IR (neat, ATR-IR): υ = 1732 cm^{-1} (C═O), 1629/1614 cm^{-1} (C═C py). HR-ESI-MS calcd for $[C_{21}H_{24}N_4O_8 + H]^+$, 461.1672; found, 461.1665, $[M + H]^+$, PPM = −1.5. Anal. Calcd for H_4C3octapa·4HCl·2H_2O ($C_{21}H_{24}N_4O_8$·4HCl·2H_2O = 642.312 g/mol): C, 40.40; H, 4.84; N, 8.97. Found: C, 40.14 (Δ = 0.26); H, 4.74 (Δ = 0.10); N, 8.84 (Δ = 0.13).

Na[In(C3octapa)] (6). H_4C3octapa·4HCl·2H_2O (**5**) (15.54 mg, 0.024 mmol) was suspended in 0.1 M HCl (1.5 mL), and $In(NO_3)_3$·6H_2O (12.9 mg, 0.031 mmol) was added. The pH was adjusted to 4−5 using 0.1 M NaOH, and then the solution was stirred at room temperature. After 1 h, the product was confirmed via mass spectrometry, and the solvent was removed in vacuo to yield Na[In(C3octapa)] (**6**). ^{1}H NMR (400 MHz, D_2O, 25 °C) δ 8.42−7.88 (m, 4H), 7.76−7.47 (m, 2H), 4.45−3.85 (m, 4H), 3.64−3.33 (m, 2H), 3.15−2.73 (m, 2H), 2.53−2.19 (m, 4H), 1.30 (m, 1H), 1.04 (m, 1H). HR-ESI-MS calcd for $[C_{21}H_{18}{}^{115}InN_4O_8 + 2H]^+$, 571.0320; found, 571.0317, $[M + 2H]^+$, PPM = −0.5.

Na[Lu(C3octapa)] (7). H_4C3octapa·4HCl·2H_2O (**5**) (15.9 mg, 0.025 mmol) was suspended in 0.1 M HCl (1.5 mL), and $Lu(NO_3)_3$·6H_2O (15.1 mg, 0.032 mmol) was added. The pH was adjusted to 4−5 using 0.1 M NaOH, and then the solution was stirred at room temperature. After 1 h, the product was confirmed via mass spectrometry, and the solvent was removed in vacuo to yield Na[Lu(C3octapa)] (**6**). ^{1}H NMR (300 MHz, D_2O, 25 °C) δ 8.22−7.66 (m, 5H), 7.36−7.22 (m, 1H), 4.54−4.38 (m, 1H), 4.22−3.85 (m, 3H), 3.58−3.21 (m, 4H), 2.81−2.32 (m, 4H), 1.87−1.64 (m, 2H).

dx.doi.org/10.1021/ic501466z | Inorg. Chem. 2014, 53, 10412−10431

HR-ESI-MS calcd for $[C_{21}H_{18}{}^{175}LuN_4O_8 + 2H]^+$, 631.0689; found, 631.0680, $[M + 2H]^+$, PPM = −1.4.

Diethyl-2-(4-nitrobenzyl)malonate (8). This synthesis was adapted from a literature preparation.[38] Sodium ethoxide (3.47 g, 50.9 mmol) was added to ethanol (100 mL), followed by slow addition of diethyl malonate (14.1 mL, 14.8 g, 92.6 mmol) and then 4-nitrobenzyl bromide (10.0 g, 46.3 mmol). The dark orange reaction mixture was heated to reflux overnight, and it was observed that a fine white precipitate formed. The volume of the reaction mixture was reduced to 20 mL, it was placed in the freezer for several hours to encourage maximum precipitation, and then the shiny white solid was isolated via suction filtration. The procedure was repeated, reducing the volume to ∼5−10 mL and then placing in the freezer to recover more product. The white solid was filtered and rinsed with cold ethanol to isolate pure **8** (3.76 g, 12.7 mmol, ∼27%). ^{1}H NMR (300 MHz, $CDCl_3$) δ 8.16 (m, 2H, NO_2-Ph-H), 7.40 (m, 2H, NO_2-Ph-H), 4.18 (m, 4H, -O-CH_2-), 2.91 (t, 1H, -CO-CH-CO, ^3J = 7.8 Hz), 3.32 (d, 2H, -CH_2-Ph-NO_2, ^3J = 7.8 Hz), 1.23 (t, 6H, -O-CH_2-CH_3-, ^3J = 7.1 Hz). ^{13}C NMR (100 MHz, CDCl3) δ 168.2, 146.9, 145.6, 129.8, 123.7, 61.8, 53.1, 34.3, 13.9. HR-ESI-MS calcd for $[C_{14}H_{17}NO_6+H]^+$, 296.1134; found, 296.1133, $[M + H^+]^+$, PPM = −0.4.

2-(4-Nitrobenzyl)malondiamide (9). Compound **8** (3.52 g, 11.9 mmol) was dissolved in methanol (125 mL) to form a clear and colorless mixture and was then placed in an ice/salt bath. After cooling, ammonia gas was purged through the reaction vessel for ∼10 min with vigorous stirring to allow for NH_3(g) saturation. After NH_3(g) saturation, the reaction mixture turned clear yellow. The ammonia gas flow was ceased, and the reaction vessel was sealed with a rubber septum and then allowed to stir in the ice bath overnight. While stirring overnight, the ice bath melted, and the reaction mixture warmed to ambient temperature. After stirring overnight, a precipitate was observed to have formed, and the reaction mixture was a yellow/orange suspension. The reaction mixture was allowed to stir at ambient temperature for a second night (∼36 h total). The precipitate was filtered out, washed with methanol followed by boiling acetonitrile, and then dried in vacuo. The product (**9**) was isolated as yellow solid (2.34 g, 9.86 mmol, ∼83%). ^{1}H NMR (300 MHz, DMSO-d_6) δ 8.15−8.12 (m, 2H, NO_2-Ph-H), 7.49−7.46 (m, 2H, NO_2-Ph-H), 7.30 (s, 2H, -NH_2), 7.08 (s, 2H, -NH_2), 3.39 (t, 1H, ^3J = 7.8 Hz, -CO-CH-CO-), 3.10 (d, 2H, ^3J = 7.6 Hz, -CH_2-Ph-NO_2-). ^{13}C NMR (75 MHz, DMSO-d_6) δ 170.1, 148.0, 146.0, 130.1, 123.2, 54.0, 34.5. HR-ESI-MS calcd for $[C_{10}H_{11}N_3O_4+Na]^+$, 260.0647; found, 260.0654, $[M + Na^+]^+$, PPM = 2.6. Anal. Calcd for $C_{10}H_{11}N_3O_4\cdot 0.1CH_3OH$ = 240.424 g/mol: C, 50.46; H, 4.78; N, 17.71. Found: C, 50.61 (Δ = 0.15); H, 4.60 (Δ = 0.18); N, 17.26 (Δ = 0.22).

1,3-Diamino-2-(4-nitrobenzyl)propane Dihydrochloride (2-(*p*-nitrobenzyl)-1,3-propylenediamine) (10). Compound **9** (1.99 g, 8.40 mmol) was added to a two-necked round-bottomed flask under argon gas, and an addition funnel was attached. Borane stabilized in THF (BH_3·THF, 1 M, 15 mL) was added, and the reaction mixture was heated to reflux under argon gas for 20 h. The reaction mixture was clear yellow with solid precipitate on the sides of the flask. The reaction mixture was removed from heat, ∼30 mL of concentrated HCl (12 M) was added slowly, and the mixture heated to reflux for ∼1 h. The reaction mixture was reduced to dryness in vacuo, and then ∼40 mL of NaOH (6 M) was added. The aqueous phase was extracted with dichloromethane (5 × 30 mL), and the light yellow organic extractions were pooled and dried over magnesium sulfate, filtered, and reduced to dryness in vacuo. The product was then suspended in ∼20 mL of ethanol, concentrated HCl was added (∼3 mL, 12 M), and the flask placed in the freezer. A light yellow precipitate formed, which was filtered out, washed with dichloromethane, and dried in vacuo to isolate pure **10** (0.544 g, 2.39 mmol, ∼28%). ^{1}H NMR (400 MHz, D_2O) δ 8.18 (m, 2H, NO_2-Ph-H (meta to NO_2)), 7.51 (m, 2H, NO_2-Ph-H (ortho to NO_2)), 3.19 (dd, 2H, H_2N-CH_2-), ^3J = 6.7 Hz, ^2J = 13.6 Hz), 3.06 (dd, 2H, H_2N-CH_2-), ^3J = 6.7 Hz, ^2J = 13.5 Hz), 2.97 (2, 2H, NO_2-Ph-CH_2-, ^3J = 7.6 Hz), 2.56 (septet, 1H, -CH-, ^3J = 6.9 Hz). ^{13}C NMR (100 MHz, D_2O) δ 146.6, 145.6, 130.4, 124.2, 40.22, 36.7, 34.9. HR-ESI-MS calcd for $[C_{10}H_{15}N_3O_2+H]^+$, 210.1214; found, 210.1240, $[M + H^+]^+$, PPM = −1.2.

***N,N′*-(2-Nitrobenzenesulfonamide)-2-(*p*-nitrobenzyl)-1,3-diaminopropane (11).** Compound **10** (205 mg, 0.979 mmol) was dissolved in THF (10 mL), and the reaction mixture placed in an ice bath. Sodium bicarbonate (∼1 g) was added, followed by the slow addition of 2-nitrobenzenesulfonyl chloride (445 mg, 2.01 mmol). The reaction mixture was stirred overnight at ambient temperature. The yellow/orange mixture was filtered to remove sodium bicarbonate, rotary evaporated to a red oil, and purified by silica chromatography (CombiFlash R_f automated column system; 40 g HP silica; A: hexanes, B: ethyl acetate, 100% A to 100% B gradient), and dried in vacuo to yield **11** as off-white solid (77%, ∼439 mg). ^{1}H NMR (300 MHz, acetone-d_6, 25 °C) δ 8.14−8.11 (m, 2H), 8.04−8.01 (m, 2H), 7.97−7.82 (m, 6H), 7.50 (d, J = 9.0 Hz, 2H), 6.76 (t, J = 8.0 Hz, 2H), 3.29−3.12 (m, 4H), 2.91 (d, J = 9.0 Hz, 2H), 2.34 (sept, J = 8.0 Hz, 1H). ^{13}C NMR (75 MHz, acetone-d_6, 25 °C) δ 149.0, 148.8, 147.5, 135.0, 133.8, 133.6, 131.4, 131.1, 125.9, 124.3, 45.0, 41.8, 35.9. HR-ESI-MS calcd for $[C_{22}H_{21}N_5O_{10}S_2+H]^+$, 580.0808; found, 580.0812 $[M + H]^+$, PPM = 0.7.

***N,N′*-(2-Nitrobenzenesulfonamide)-*N,N′*-[(*tert*-butoxycarbonyl)methyl]-2-(*p*-nitrobenzyl)-1,3-diaminopropane (12).** To a solution of **11** (195 mg, 0.336 mmol) in dimethylformamide (5 mL, dried over molecular sieves 4 Å) were added *tert*-butylbromoacetate (109 μL, 0.740 mmol) and sodium carbonate (∼400 mg). The yellow reaction mixture was stirred at 50 °C overnight, filtered to remove sodium carbonate, and concentrated in vacuo. The crude product was purified by silica chromatography (CombiFlash R_f automated column system; 40 g HP silica; A: ethyl acetate, B: petroleum ether, 100% A to 100% B gradient) to yield **12** as light yellow fluffy solid (83%, ∼224 mg). ^{1}H NMR (300 MHz, $CDCl_3$, 25 °C) δ 8.11 (d, J = 8.0 Hz, 2H), 7.92−7.90 (m, 2H), 7.67 (m, 4H), 7.58−7.55 (m, 2H), 7.38 (d, J = 9.0 Hz, 2H), 4.08−3.93 (m, 4H), 3.55 (dd, J = 13.5 Hz, J = 9.0 Hz, 2H), 3.23 (dd, J = 13.5 Hz, J = 9.0 Hz, 2H), 2.89 (d, J = 9.0 Hz, 2H), 2.46 (sept, J = 8.0 Hz, 1H), 1.26 (s, 18H). ^{13}C NMR (75 MHz, $CDCl_3$, 25 °C) δ 167.1, 147.9, 147.4, 146.5, 133.7, 132.7, 132.2, 131.7, 130.8, 129.7, 123.9, 123.6, 82.5, 50.9, 49.6, 38.0, 36.4, 27.6. HR-ESI-MS calcd for $[C_{34}H_{41}N_5O_{14}S_2+Na]^+$, 830.1989; found, 830.1996, $[M + Na]^+$, PPM = 0.8.

***N,N′*-[(*tert*-Butoxycarbonyl)methyl]-2-(*p*-nitrobenzyl)-1,3-diaminopropane (13).** To a solution of **12** (224.4 mg, 0.278 mmol) in tetrahydrofuran (5 mL) were added thiophenol (58.2 μL, 0.569 mmol) and potassium carbonate (excess, ∼0.4 g). The reaction mixture was stirred at ambient temperature for 72 h as a slow color change from light yellow to dark yellow occurred. The crude reaction mixture was filtered out with a large fritted glass filter, rinsed liberally with THF and CH_3CN, and then concentrated to dryness in vacuo. The resulting crude yellow oil was purified by silica chromatography (CombiFlash R_f automated column system; 24 g HP silica; A: dichloromethane, B: methanol, 100% A to 30% B gradient) to yield **13** as clear yellow oil (90%, ∼109 mg). ^{1}H NMR (300 MHz, $CDCl_3$, 25 °C) δ 8.08 (d, J = 9.0 Hz, 2H), 7.32 (d, J = 9.0 Hz, 2H), 3.20 (s, 4H), 2.74 (d, J = 8.0 Hz, 2H), 2.53 (d, J = 8.0 Hz, 4H), 1.93 (m, 1H), 1.85 (s, 2H), 1.39 (s, 18H). ^{13}C NMR (75 MHz, $CDCl_3$, 25 °C) δ 171.6, 148.6, 146.2, 129.8, 123.3, 80.9, 51.8, 51.5, 40.8, 36.8, 27.9. HR-ESI-MS calcd for $[C_{22}H_{35}N_3O_6+H]^+$, 438.2604; found, 438.2593, $[M + H]^+$, PPM = −2.5.

***N,N′*-[(*tert*-Butoxycarbonyl)methyl]-*N,N′*-[(6-methoxycarbonyl)pyridin-2-yl)methyl]-2-(*p*-nitrobenzyl)-1,3-diaminopropane (14).** To a solution of **13** (52.2 mg, 0.119 mmol) in acetonitrile (5 mL) were added methyl 6-(bromomethyl)-picolinate[14] (57.6 mg, 0.251 mmol) and sodium carbonate (∼200 mg). The reaction mixture was stirred at 60 °C overnight. Sodium carbonate was removed by filtration, and the crude mixture was concentrated in vacuo. The crude oil was purified by column chromatography (CombiFlash R_f automated column system; 24 g HP silica; A: dichloromethane, B: methanol, 100% A to 20% B gradient) to afford **14** as light yellow oil (95%, ∼83.6 mg). ^{1}H NMR (300 MHz, $CDCl_3$, 25 °C) δ 8.00 (dd, J = 8.5 Hz, J = 19.5 Hz, 4H), 7.70−7.70 (m, 4H), 7.21 (d, J = 9 Hz, 2H), 3.95 (s, 6H, methyl ester), 3.90 (s, 4H), 3.16 (s, 4H), 2.74−2.66 (m, 4H), 2.45−2.38 (m, 2H), 1.95 (m, 1H), 1.38 (s, 18H). ^{13}C NMR (75 MHz, $CDCl_3$, 25 °C) δ

dx.doi.org/10.1021/ic501466z | Inorg. Chem. 2014, 53, 10412−10431

170.1, 165.6, 160.4, 149.2, 147.2, 146.1, 137.3, 129.7, 126.0, 123.6, 123.3, 81.0, 60.8, 57.5, 56.7, 52.8, 37.9, 37.3, 28.0. HR-ESI-MS calcd for $[C_{38}H_{49}N_5O_{10}+H]^+$, 736.3558; found, 736.3575, $[M + H]^+$, PPM = 2.3.

***p*-SCN-Bn-H$_4$C3octapa, *N,N′*-[(Carboxylato)methyl]-*N,N′*-[(6-carboxylato)pyridin-2-yl)methyl]-2-(*p*-benzyl-isothiocyanato)-1,3-diaminopropane (15).** Compound **14** (92.4 mg, 0.126 mmol) was dissolved in glacial acetic acid (2.5 mL) with hydrochloric acid (2.5 mL, 3 M). Palladium on carbon (10 wt %) was added, and hydrogen gas (balloon) was purged through the reaction vessel that was then sealed with a rubber septum. The reaction mixture was stirred vigorously at ambient temperature for 1 h and then filtered to remove Pd/C and washed ad libitum with methanol and hydrochloric acid (3 M). The crude reaction mixture was concentrated in vacuo, dissolved in a mixture of tetrahydrofuran/deionized water (3:1, 5 mL), LiOH (150 mg) was added, and the mixture was stirred at ambient temperature for 1 h. The crude reaction mixture was dissolved in hydrochloric acid (~2 mL, 3 M), heated to near boiling with a heat gun to affect full *tert*-butyl ester deprotection, and then allowed to cool to ambient temperature. The crude reaction mixture was then mixed with thiophosgene (purchased suspended in chloroform) in ~0.2 mL of additional chloroform (15 equiv, 144 μL, 1.88 mmol) to react overnight at ambient temperature with vigorous stirring. The reaction mixture was washed with chloroform (5 × 1 mL) by vigorous biphasic stirring, followed by removal of the organic phase using a pipet to extract excess thiophosgene. The aqueous phase was then diluted to a volume of 4.5 mL with deionized water and injected directly onto a semiprep HPLC column for purification (A: 0.1% TFA in deionized water, B: 0.1% TFA in CH_3CN, 100% A to 60% B gradient over 40 min). *p*-SCN-Bn-H$_4$C3octapa (**15**) was found in the largest peak at t_R = 35 min (broad), lyophilized overnight, and was isolated as a fluffy off-white solid (53% over three steps from **15**, ~40 mg). ^{1}H NMR (400 MHz, MeOD, 25 °C) δ 8.06−8.03 (m, 2H), 7.91 (t, J = 7.9 Hz, 2H), 7.55−7.53 (m, 2H), 7.27 (d, J = 8.6 Hz, 2H), 7.16 (d, J = 8.2 Hz, 2H), 4.70 (d, J = 7.3 Hz, 2H), 4.48 (d, J = 14.3 Hz, 2H), 4.19 (d, J = 17.7 Hz, 2H), 3.84 (d, J = 17.7 Hz, 2H), 3.44 (d, J = 12.0 Hz, 2H), 3.28 (d, J = 12.6 Hz, 2H), 2.94 (m, 1H), 2.61 (d, J = 7.2 Hz, 2H). ^{13}C NMR (100 MHz, MeOD, 25 °C) δ 171.7, 167.4, 155.0, 149.7, 139.9, 139.5, 137.1, 131.8, 139.5, 129.4, 126.9, 126.1, 61.2, 58.7, 55.3, 37.2, 33.3. IR (neat, ATR-IR): υ = 2097 cm^{-1} (S═C═N-), 1718/1661 cm^{-1} (C═O), 1594 cm^{-1} (C═C py). HR-ESI-MS calcd for $[C_{29}H_{29}N_5O_8S+H]^+$, 608.1815; found, 608.1822, $[M + H]^+$, PPM = 1.2.

Molecular Modeling. Calculations were performed using the Gaussian 09[39] and GaussView packages. Molecular geometries and electron densities were obtained from density functional theory calculations, with the B3LYP functional employing the 6-31+G(d,p) basis set for first- and second-row elements, and the Stuttgart/Dresden and associated ECP's basis set was employed for the metals, lutetium and indium.[40,41] Solvent (water) effects were described through a continuum approach by means of the IEF PCM as implemented in G09. The electrostatic potential was mapped onto the calculated electron density surface. The corresponding harmonic vibration frequencies were computed at the same level to characterize the geometry as a minimum.

Solution Thermodynamics. The experimental procedures and details of the apparatus closely followed our reported studies of H$_2$dedpa/Ga^{3+}, and H$_4$octapa with In^{3+}, Lu^{3+}, and Y^{3+}.[14,15,28,42] As a result of the strength of the binding of the In^{3+} and Lu^{3+} complexes [In(C3octapa)]$^-$ and [Lu(C3octapa)]$^-$, the complex formation constant with this ligand could not be determined directly, and ligand−ligand competition using the known competitor, Na$_2$H$_2$EDTA, was employed. Potentiometric titrations were performed using a Metrohm Titrando 809 equipped with a Ross combination pH electrode and a Metrohm Dosino 800. Data were collected in triplicate using PC Control (version 6.0.91, Metrohm). The titration apparatus consisted of a water-jacketed glass vessel maintained at 25.0 (±0.1 °C, Julabo water bath). Prior to and during the course of the titration, a blanket of nitrogen, passed through 10% NaOH to exclude any CO_2, was maintained over the sample solution. Indium and lutetium ion solutions were prepared by dilution of the appropriate atomic absorption standard (AAS) solution. The exact amount of acid present in the indium and lutetium standard was determined by separate titrations of equimolar solutions of In^{3+} or Lu^{3+} and Na$_2$H$_2$EDTA. The amount of acid present was determined by Gran's method.[43] Calibration of the electrode was performed prior to each measurement by titrating a known amount of HCl with 0.1 M NaOH. Calibration data were analyzed by standard computer treatment provided within the program MacCalib[44] to obtain the calibration parameters E_0. Ligand solutions were prepared 24 h in advance of titrations to allow for equilibration. Electrode equilibration times for titrations were up to 10 min for pK_a titrations and up to 3 h for metal complex titrations (<0.2 mV/min drift allowed). Ligand and metal concentrations were 0.75−1.0 mM for potentiometric titrations. The data were treated with Hyperquad2008.[45] The proton dissociation constants corresponding to hydrolysis of In^{3+}(aq) and Lu^{3+}(aq) ions included in the calculations were taken from Baes and Mesmer.[46] The K_{ML} value for the indium−EDTA and lutetium−EDTA complexes was taken from Martell. Values of pM were calculated under physiologically relevant conditions of pH 7.4, 10 μM ligand, and 1 μM metal. All values and errors represent the average of at least three independent experiments.

Trastuzumab Antibody Modification/Thiourea Bioconjugation. Trastuzumab (purchased commercially as Herceptin, Genentech, San Francisco, CA) was purified using centrifugal filter units with a 50 000 molecular weight cutoff (Amicon ultra centrifuge filters, Ultracel-50: regenerated cellulose, Millipore Corp., Billerica, MA) and phosphate buffered saline (PBS, pH 7.4) to remove α-α-trehalose dihydrate, L-histidine, and polysorbate 20 additives. After purification, the antibody was taken up in PBS, pH 7.4. Subsequently, 300 μL of antibody solution (150−250 μM) was combined with 100 μL of PBS (pH 8.0); the pH of the resulting solution was adjusted to 8.8−9.0 with 0.1 M Na_2CO_3, and 4 equiv of the *p*-SCN-Bn-H$_4$C3octapa or *p*-SCN-Bn-H$_4$octapa was added in 10 μL DMSO. The reactions were incubated at 37 °C for 1 h, followed by centrifugal filtration to purify the resultant antibody conjugate. The final modified antibody stock solutions were stored in PBS (pH 7.4) at 4 °C.

^{111}In- and ^{177}Lu-C3octapa/octapa−Trastuzumab Radiolabeling. Aliquots of H$_4$C3octapa/H$_4$octapa−trastuzumab immunoconjugates (~400 μg) were transferred to 2 mL microcentrifuge tubes and made up to 1 mL of ammonium acetate buffer (pH 5.5, 200 mM), and then aliquots of ^{177}Lu or ^{111}In were added (~2−3 mCi). The H$_4$octapa−trastuzumab mixtures were allowed to radiolabel at room temperature for 30 min and then analyzed via iTLC with an eluent of 50 mM EDTA (pH 5) and confirmed reproducible values >95% RCY, with ^{111}In being ~94−95% (~2.23 mCi/mg) and ^{177}Lu being ~97−98% (~2.52 mCi/mg) (Figures S21−S24). The H$_4$C3octapa−trastuzumab mixtures were allowed to radiolabel at room temperature for 60 min and then analyzed via iTLC with RCY for ^{111}In of ~95−96% (~2.25 mCi/mg) and RCY of ^{177}Lu of ~8−9% (~0.3 mCi/mg). The low radiolabeling yield for ^{177}Lu appears to be due to immediate transchelation of ^{177}Lu to the iTLC EDTA mobile phase, suggesting poor stability of the H$_4$C3octapa complex. EDTA solution (30 μL, 50 mM, pH 5) was then added to the reaction mixture; the resultant radiolabeled immunoconjugates were then purified using size-exclusion chromatography (Sephadex G-25 M, PD-10 column, 30 kDa, GE Healthcare; dead volume = 2.5 mL, eluted with 1 mL fractions of PBS, pH 7.4) and centrifugal column filtration (Amicon ultra 50k MWCO). The radiochemical purity of the final radiolabeled bioconjugate was assayed by radio-iTLC and was found to be >99% for both H$_4$octapa−trastuzumab samples (Figures S21−24), but for ^{111}In-C3octapa−trastuzumab a small amount of ^{111}In was transchelated by the EDTA mobile phase after purification (Figures S21−24), and for ^{177}Lu−C3octapa−trastuzumab, a very substantial amount of ^{177}Lu was leached out of the ligand and transchelated by the EDTA mobile phase (Figures S21−24). In the iTLC experiments, ^{111}In- and ^{177}Lu-octapa/DOTA−trastuzumab remained at the baseline, whereas ^{177}Lu^{3+}/^{111}In^{3+} ions complexed as [^{111}In/^{177}Lu]−EDTA eluted with or near the solvent front.

dx.doi.org/10.1021/ic501466z | Inorg. Chem. 2014, 53, 10412−10431

Scheme 1. Synthesis of H_4C3octapa (5) Utilizing Nosyl Protection Chemistry[a]

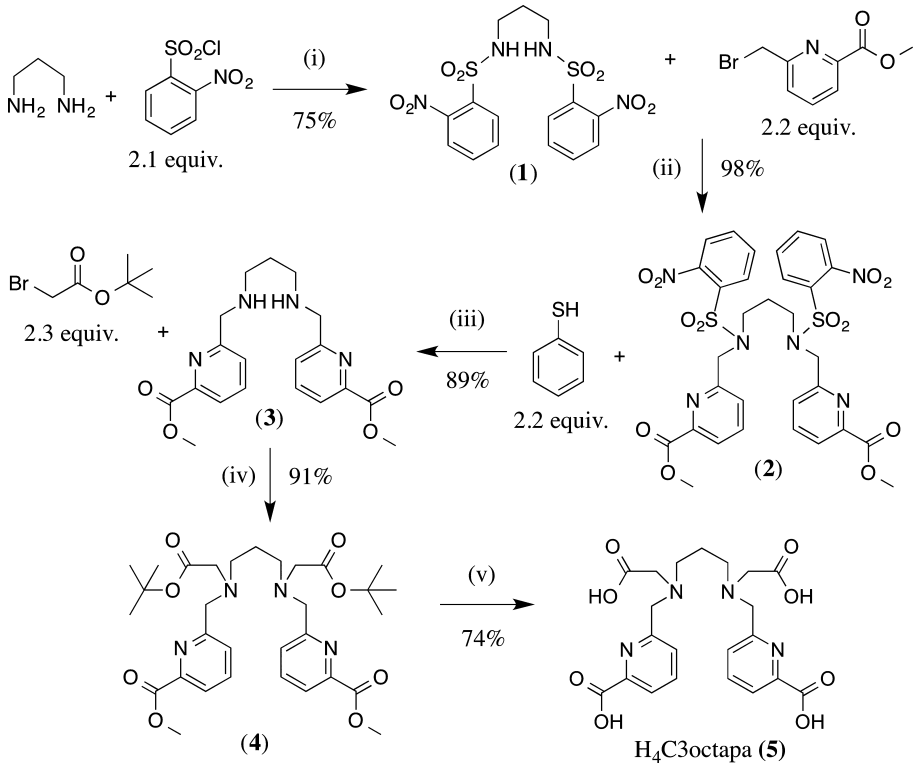

[a](i) THF, $NaHCO_3$ (excess), 2-nitrobenzenesulfonyl chloride, 0 °C → RT, 20 h (**1**); (ii) DMF, Na_2CO_3 (excess), methyl-6-bromomethylpicolinate, 50 °C, 20 h (**2**); (iii) THF, thiophenol, K_2CO_3 (excess), RT, 72 h (**3**); (iv) CH_3CN, Na_2CO_3 (excess), *tert*-butylbromoacetate, 60 °C, 20 h (**4**); (v) THF/H_2O (3:1), LiOH, RT, 4 h (H_4C3octapa, **5**). Cumulative yield of ∼44% in five steps.

^{111}In- and ^{177}Lu-C3octapa/octapa−Trastuzumab Blood Serum Competition Experiments. Frozen human blood serum was thawed for 30 min, and 300 μL aliquots were transferred to 2.0 mL Corning centrifuge vials. A portion of radiolabeled immunoconjugate (∼50 μg, ∼400 μCi) was transferred to the blood serum. Serum competition samples were then incubated at 37 ± 0.1 °C with gentle agitation (300 rpm) and analyzed via iTLC with an EDTA eluent (50 mM, pH 5.0) (Bioscan AR-2000) at time points of 0, 24, 48, 72, 96, and 120 h.

[^{177}Lu(chelate)] Radiolabeling and Serum Stability. For ^{177}Lu experiments with nonbifunctional ligands, the ligands H_4octapa, H_4C3octapa, DTPA, and DOTA were used. Aliquots of each chelator stock solution (1 mg/mL) were transferred to Corning 2.0 mL self-standing microcentrifuge tubes containing ∼1.2 mCi of ^{177}Lu to a ligand concentration of ∼180 μM and made up to 1 mL with NaOAc buffer (10 mM, pH 5.0). H_4octapa, H_4C3octapa, and DTPA were allowed to radiolabel at ambient temperature for 10 min, and DOTA was radiolabeled for 1 h at 90 °C. Radiometal complexes were then evaluated using radio-HPLC to confirm quantitative radiometal coordination (linear gradient A: 0.1% TFA in H_2O, B: CH_3CN, 0−80% B over 30 min). Radiolabeled ligands were then used for blood serum stability assays. Frozen human blood serum was thawed for 30 min, and 750 μL aliquots were transferred to 2.0 mL Corning centrifuge vials. Three hundred microliters of each ^{177}Lu(chelate) was transferred to 750 μL of blood serum along with 450 μL of PBS to a total volume of 1.5 mL (n = 3 for each ligand). The final ^{177}Lu(chelate) concentration present in serum was ∼36 μM. Serum competition samples were then incubated at 37 ± 0.1 °C with constant agitation (550 rpm) and analyzed via PD-10 size-exclusion column elution (filters MW < 5000 Da) at 1.5 and 24 h time points and counted using a Capintec CRC-15R dose calibrator. Aliquots of 500 μL of each serum/^{177}Lu(chelate) competition solution (n = 3) were removed from the competition vial, diluted to 2.5 mL with PBS, and counted. The diluted aliquot of serum competition mixture was loaded onto a conditioned PD-10 column. The loading volume (2.5 mL) was eluted into radioactive waste, and then an additional 3.5 mL of PBS was loaded, collected, and counted in the dose calibrator as the serum-bound ^{177}Lu (nonchelate bound). Percent stability was reported as a percentage of ^{177}Lu still chelate-bound and not associated with serum proteins (MW < 5000 Da). Data is shown in Table 3. In previous work, free radiometal (^{111}In) was loaded onto a PD10 column in the same manner as described above, and it was found that no activity was eluted.[14] Additionally, ^{111}In was added directly to a mixture of mouse serum, loaded onto a PD10 column, and it was found that no activity was retained on the column after elution.[14]

RESULTS

Synthesis and Characterization. The ligand H_4C3octapa and its bifunctional derivative *p*-SCN-Bn-H_4C3octapa were synthesized for the first time using a synthetic route similar to a recently developed method for H_4octapa (Scheme 1).[28] Although the synthesis of *p*-SCN-Bn-H_4octapa utilizes the enantiopure starting material L-4-nitrophenylalanine, for *p*-SCN-Bn-H_4C3octapa a different synthesis was used, starting from diethylmalonate and 4-nitrobenzyl bromide, so that a single additional carbon atom could be inserted to obtain a symmetric propylene bridged backbone (Scheme 2).[15,47,14,38] The 2-nitrobenzenesulfonamide (nosyl) amine-protecting group has made the synthesis of picolinic acid-based ligands higher yielding and more efficient.[28,42,48−53] Synthesis of H_4C3octapa was completed in five steps with a cumulative yield of ∼44%, and *p*-SCN-Bn-H_4C3octapa, in seven steps with a cumulative yield of ∼29% (not including synthesis of the backbone diamine fragment).

Following ligand synthesis and purification, portions of the pure H_4C3octapa·4HCl·2H_2O salt (formula determined by

dx.doi.org/10.1021/ic501466z | Inorg. Chem. 2014, 53, 10412−10431

Scheme 2. Synthesis of *p*-SCN-Bn-H_4C3octapa (15) Utilizing Nosyl Protection Chemistry[a]

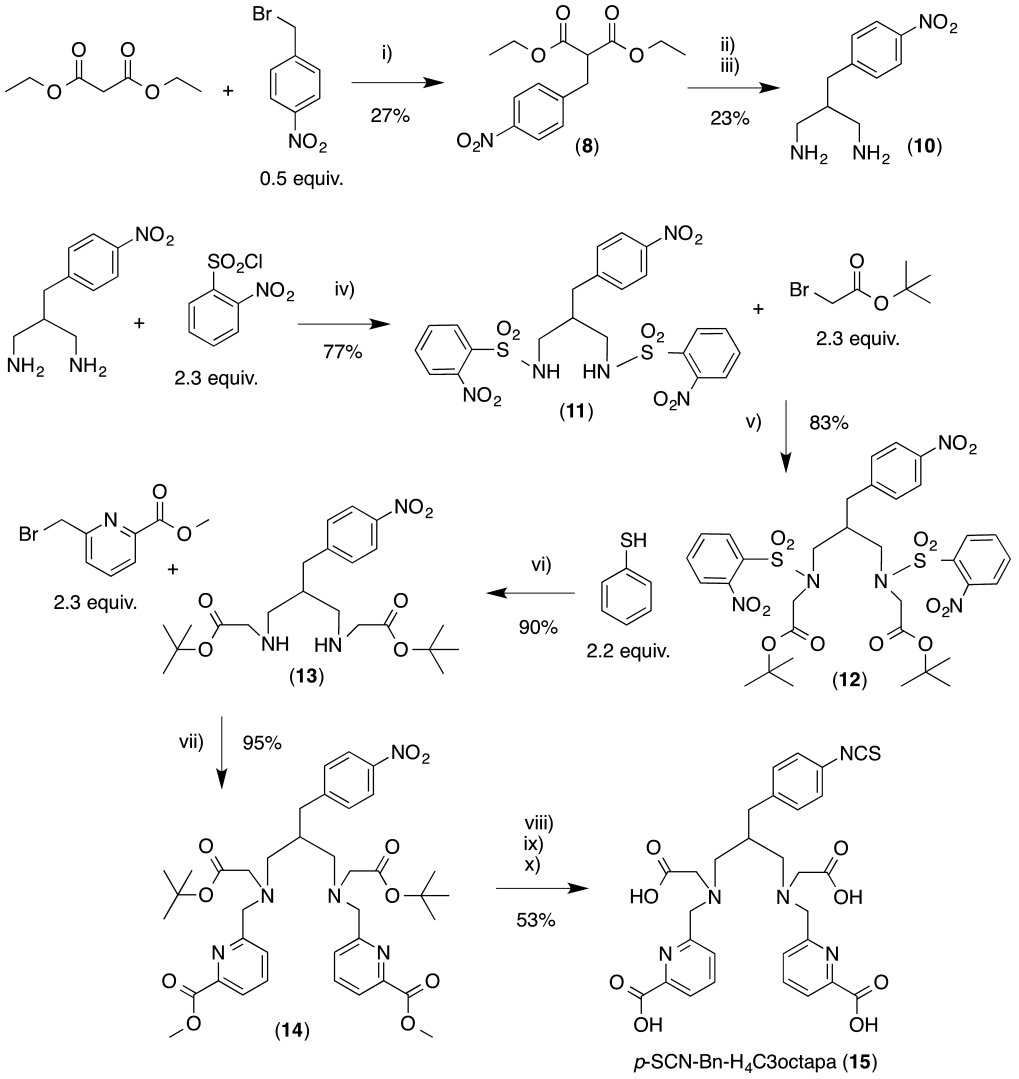

[a](i) EtOH, NaOEt, Δ, 20 h (**8**); (ii) MeOH, NH_3(g), 0 °C → RT, 36 h ; (iii) BH_3·THF, Δ, Ar(g), 20 h (**10**); (iv) THF, $NaHCO_3$ (excess), 0 °C → RT, 20 h (**11**); (v) DMF, Na_2CO_3 (excess), 50 °C, 20 h (**12**); (vi) THF, K_2CO_3 (excess), RT, 72 h (**13**); (vii) CH_3CN, Na_2CO_3 (excess), 60 °C, 20 h (**14**); (viii) 5 mL of (1:1) AcOH (glacial)/HCl (3 M), Pd/C (10 wt %), H_2(g), RT, 1 h; (ix) THF/H_2O (3:1), LiOH, RT, 4 h; (x) thiophosgene in $CHCl_3$ (15 equiv), HCl (3 M), RT, 20 h (*p*-SCN-Bn-H_4C3octapa, **15**). Cumulative yield of ∼29% in seven steps.

elemental analysis) were mixed separately with both indium nitrate [$In(NO_3)_3$·$6H_2O$] and lutetium nitrate [$Lu(NO_3)_3$·$6H_2O$] to form the coordination complexes. These metal ion complexes were characterized using standard ^{1}H NMR and HR-ESI-MS techniques, 2D ^{1}H−^{1}H COSY and ^{1}H−^{13}C HSQC NMR, and variable temperature (VT) NMR spectroscopy. Due to the presence of multiple isomers formed under aqueous conditions for [In(C3octapa)]$^-$ and [Lu(C3octapa)]$^-$, and fluxional isomerization observed for [Lu(C3octapa)]$^-$ at ambient temperature, complete ^{13}C NMR spectra could not be obtained in a reasonable time (e.g., no suitable spectrum for ^{13}C NMR, 150 MHz, 20 h acquisition). 2D-HSQC heteronuclear single bond correlation experiments provide more sensitive acquisition of ^{13}C signals than do standard ^{13}C NMR experiments, so because of the difficulty obtaining complete ^{13}C NMR spectra, HSQC spectra were obtained in their place. It is important to note that the different isomers of these metal complexes could not be separated during purification by semipreparative reverse-phase high-performance liquid chromatography, as the complexes eluted as single broad peaks, as did the previously studied [In(octapa)]$^-$, [Lu(octapa)]$^-$, and [Y(octapa)]$^-$ complexes.[14,28,42]

^{1}H NMR Spectroscopy of [In(C3octapa)]$^-$ and [Lu(C3octapa)]$^-$ Compared to that of [In(octapa)]$^-$ and [Lu(octapa)]$^-$. The previously studied compound, *p*-SCN-Bn-H_4octapa, is asymmetric and contains a single stereocenter, which results in weak nuclear magnetic resonance (NMR) spectra with complicated coupling patterns, making NMR characterization challenging.[28] In contrast, *p*-SCN-Bn-H_4C3octapa contains no stereocenters and retains ∼C_2 symmetry, which results in simpler coupling patterns, easier interpretation of NMR spectra, and faster spectral acquisition (Figures S8−S10). The nonbifunctional ligands H_4octapa and H_4C3octapa both possess ∼C_{2v} symmetry, but when they are complexed to metal ions such as In^{3+} and Lu^{3+}, they show substantial changes in coupling patterns and chemical shifts.

The [C3octapa]$^{4-}$ metal ion complexes with In^{3+} and Lu^{3+} were compared to the analogous [octapa]$^{4-}$ complexes to

dx.doi.org/10.1021/ic501466z | *Inorg. Chem.* 2014, 53, 10412−10431

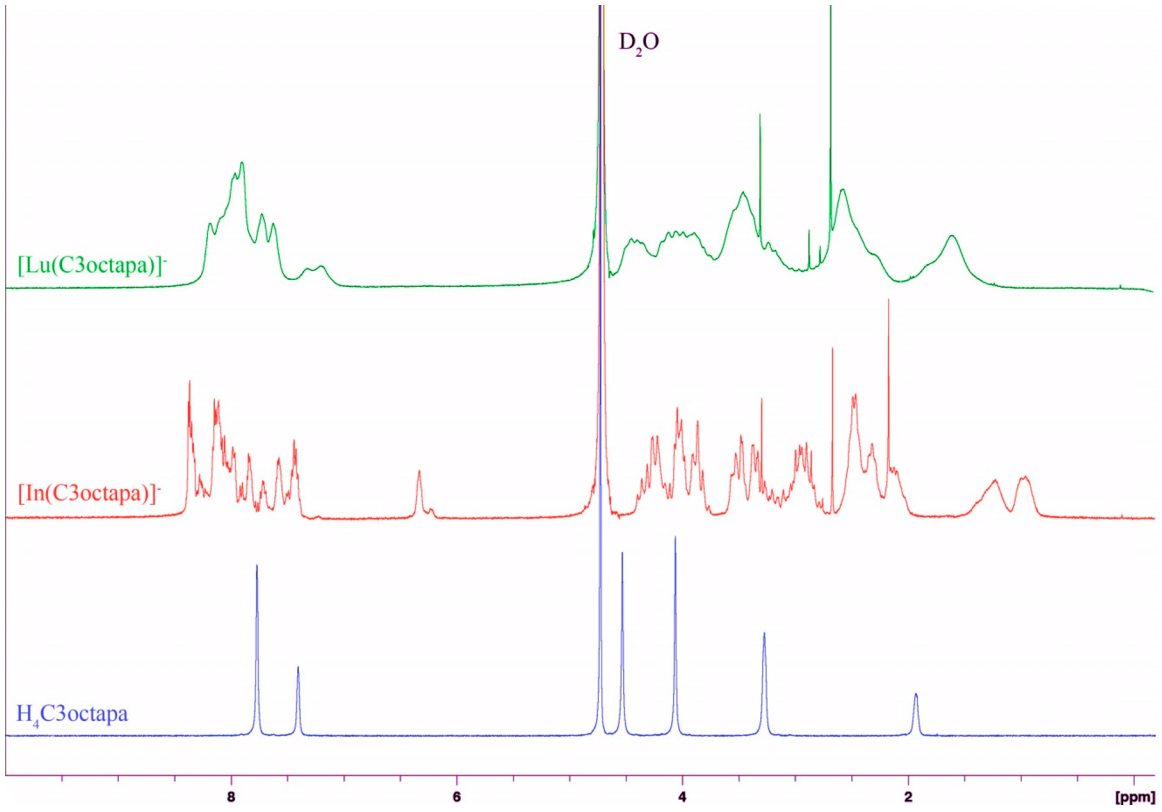

Figure 1. Stacked NMR spectra of H_4C3octapa (D_2O, 25 °C, 600 MHz), metal complex $[In(C3octapa)]^-$ (D_2O, 25 °C, 400 MHz) showing complicated but sharp signals suggesting multiple static isomers, and $[Lu(C3octapa)]^-$ (D_2O, 25 °C, 300 MHz) showing complicated and broad signals suggesting fluxional isomerization.

compare the differences between the coordination chemistry of these two structurally similar ligands. A comparison of Figures 1 and 2 highlights a large difference in the NMR spectra of the In^{3+} and Lu^{3+} metal complexes of $[C3octapa]^{4-}$ and $[octapa]^{4-}$, despite these ligands only differing by a single backbone carbon. H_4C3octapa forms a 6-membered chelate ring when coordinated to metal ions, whereas H_4octapa forms only 5-membered chelate rings. It is established that 5-membered chelate rings are generally more thermodynamically favorable than 6-membered rings for large metal ions, so this small structure difference between ligands (ethylene vs propylene bridge) is expected to impact stability to an extent.[11] The metal ion complexes of H_4octapa (Figure 2) display less isomerization and fluxionality than do those of H_4C3octapa (Figure 1), with the $[In(octapa)]^-$ complex showing only 1 static isomer at ambient temperature, where the ^{1}H NMR spectrum of $[In(C3octapa)]^-$ shows a complicated set of sharp peaks, suggesting the presence multiple static isomers at ambient temperature. The contrast between Lu^{3+} complexes is similar, with the ^{1}H NMR spectrum of $[Lu(C3octapa)]^-$ showing broad signals suggesting fluxional isomerization between multiple isomers at ambient temperature (slow on the NMR time scale), whereas $[Lu(octapa)]^-$ shows sharp and well-resolved ^{1}H NMR peaks, suggesting the presence of multiple static isomers at ambient temperature.

The ethylene protons of H_4octapa originally appear as a single multiplet at ~3.0 ppm (Figure 2), but these signals in the $[Lu(octapa)]^-$ complex appear as two broad multiplets at ~2.0−2.5 ppm (~50:50 integration, Figure 2), suggesting the presence of at least two isomers. On the basis of these observations, H_4octapa appears to form In^{3+} and Lu^{3+} complexes with less fluxionality and fewer isomers than the analogous H_4C3octapa complexes, suggesting that the extra carbon present in H_4C3octapa results in a more flexible backbone and a lower energetic barrier to interconversion between isomers. Because these ligands are studied with the long-term goal of being used in radiopharmaceutical agents, it would be logical that more inert and static complexes such as those formed by H_4octapa would be favorable in order to maximize stability and inertness in vivo.

2D COSY and HSQC NMR Spectroscopy of $[In(C3octapa)]^-$ and $[Lu(C3octapa)]^-$. The ^{1}H NMR spectra of $[In(C3octapa)]^-$ and $[Lu(C3octapa)]^-$ revealed substantially more complicated splitting patterns than did the spectra of the analogous H_4octapa complexes and thus required the 2D NMR techniques ^{1}H−^{1}H COSY and ^{1}H−^{13}C HSQC to provide information on the number of isomers present. Due to the solution behavior of these metal complexes showing fluxional isomerization or the presence of multiple isomers, ^{13}C NMR spectra were not obtained, as the sensitivity was very poor (e.g., no usable ^{13}C spectrum after 20 h at 150 MHz). In order to gain more insight into the type of isomerization occurring with these metal complexes, 2D-COSY NMR experiments were performed to assess the ^{1}H−^{1}H correlations.

It can be observed in the ^{1}H NMR spectrum of $[In(C3octapa)]^-$ (Figure 1) that the signal arising from the central propylene-bridge $-CH_2-$ changed from a singlet in the free ligand at ~1.9 ppm (integration of 2H) to two broad signals at ~0.9 and ~1.3 ppm (total integration of 2H, ~50% for each peak), which show no correlation to each other in the COSY spectra (see red arrows, Figures 3 and S4). The splitting of this ^{1}H NMR singlet into two broad peaks upon In^{3+} coordination suggest that at least two major isomers are

dx.doi.org/10.1021/ic501466z | Inorg. Chem. 2014, 53, 10412−10431

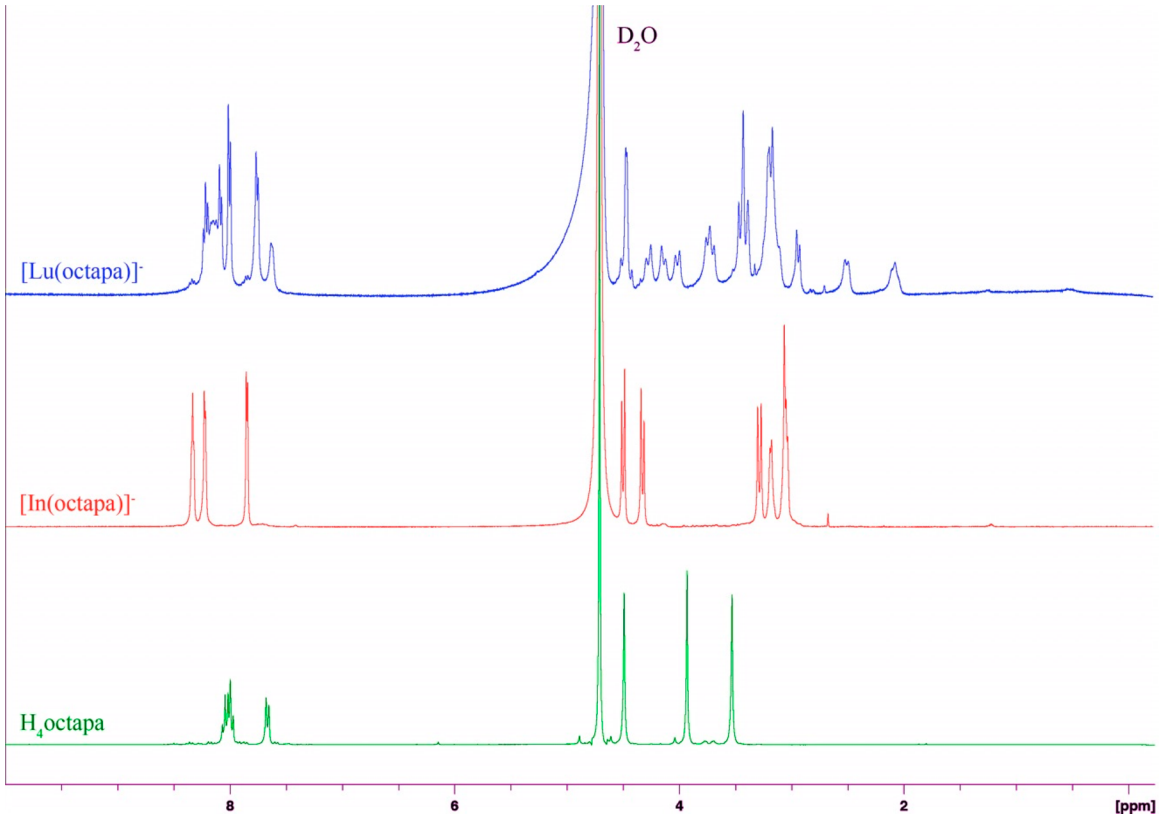

Figure 2. Stacked ^{1}H NMR spectra of H_4octapa (D_2O, 25 °C, 300 MHz), metal complex [In(octapa)]$^-$ (D_2O, 25 °C, 600 MHz) showing simple and sharp diastereotopic splitting suggesting the presence of one static isomer, and [Lu(octapa)]$^-$ (D_2O, 25 °C, 400 MHz) showing complicated and sharp signals suggesting multiple static isomers.

formed (~50:50), and the lack of correlation between these two peaks in the COSY NMR suggests that they arise from chemically distinct isomers in solution (Figure 3). The ^{1}H NMR signal arising from the central propylene-bridge CH_2 of [Lu(C3octapa)]$^-$ was observed as a single broad signal (Figure 1) rather than two broad signals, as observed for [In(C3octapa)]$^-$ (Figures 1 and 3), most likely due to signal averaging from a faster rate of fluxional isomerization at ambient temperature.

In addition to COSY experiments, 2D-HSQC heteronuclear single bond correlation (^{1}H−^{13}C) NMR spectra were obtained, which utilized an interesting diagnostic handle to assess isomerization via the ^{1}J C−H correlations of the pyridine rings (Figure 4). As previously mentioned, the 2D-HSQC experiments were more sensitive than standard ^{13}C experiments, allowing for detection of ^{13}C signals via ^{1}H−^{13}C cross-peaks. The 2D-HSQC ^{1}H−^{13}C experiments revealed a complicated set of cross-peaks arising from multiple static isomers, with the aromatic C−H pyridine signals being the most diagnostic and simple to evaluate. In the case of the free ligand or a single metal−ligand isomer, 6 carbon signals (3 if C_{2v} symmetric) should be observed in the HSQC spectra arising from the ^{1}J C−H pyridine ring correlations of the 3 aromatic C−H groups on each pyridine ring. It was observed in the HSQC spectra of [In(C3octapa)]$^-$ that 13 unique ^{13}C signals were detected, suggesting that at least 2 major isomers were present and possibly 1 minor isomer (Figure 4). If minor isomers are present, then the additional signals may have been too weak to observe from this experiment. The number of alkyl-region C−H correlations in the HSQC spectrum of [In(C3octapa)]$^-$ reveals correlations to at least 17 unique carbon atoms, with each single molecule possessing only 7 alkyl-region carbon atoms (Figure S17). Because 14 unique carbon atoms would be expected to arise from two unique isomers, this observation suggests that there are more than 2 static isomers present in aqueous solution, with the most likely explanation being two major isomers (~50:50 ratio) and one or more minor isomers.

The COSY (Figures S15 and S16) and HSQC spectral signals of [Lu(C3octapa)]$^-$ were substantially weaker than those of [In(C3octapa)]$^-$, as would be expected due to the increased rate of fluxional behavior of the Lu^{3+} complex at ambient temperature, as demonstrated by the broad ^{1}H spectrum at 25 °C (Figures 1 and 5). The HSQC spectrum of [Lu(C3octapa)]$^-$ was poorly resolved, with 10 unique carbons being observed in the aromatic region, which corresponded to pyridine C−H carbons, suggesting the presence of at least 2 fluxional isomers in solution at ambient temperature (Figure 5). The higher rate of fluxional isomerization and the coalescence of NMR signals observed for [Lu(C3octapa)]$^-$ explains why fewer ^{13}C NMR signals were detected relative to those of [In(C3octapa)]$^-$ (Figure 4 vs 5). 2D-HMBC heteronuclear multiple bond correlation NMR experiments were also performed; however, after 10−12 h of acquisition time, the spectral signals obtained were too weak to evaluate (~15 mg of compound in ~300 μL of D_2O, 600 mHz).

Variable Temperature (VT) ^{1}H NMR of [In(C3octapa)]$^-$ and [Lu(C3octapa)]$^-$. In order to gain more insight into the solution chemistry of these metal complexes, variable temperature (VT) ^{1}H NMR experiments were performed with [In(C3octapa)]$^-$ and [Lu(C3octapa)]$^-$. At 85 °C (maximum

dx.doi.org/10.1021/ic501466z | Inorg. Chem. 2014, 53, 10412−10431

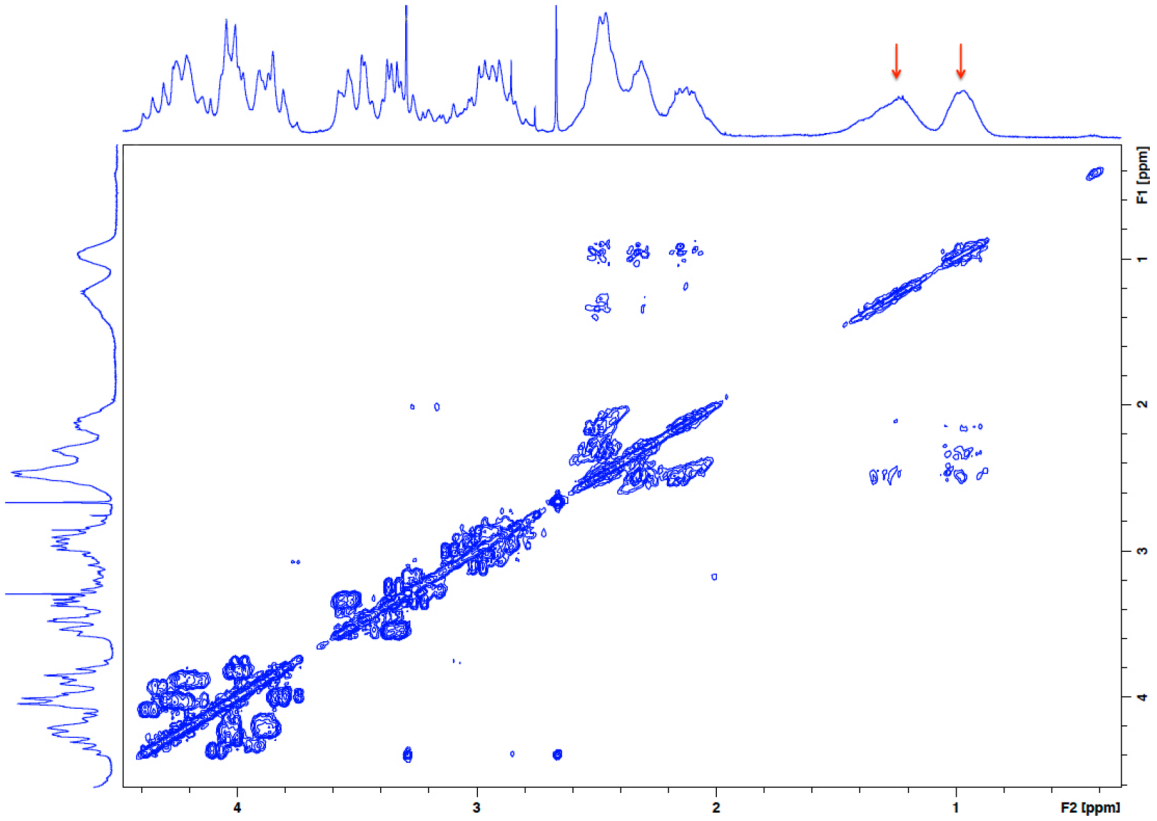

Figure 3. ^{1}H−COSY NMR (400 mHz, D_2O, 25 °C) spectrum of [In(C3octapa)]$^{-}$ showing an expansion of the alkyl-region, highlighting two broad signals with red arrows arising from the central $-CH_2-$ of the propylene bridge, showing no ^{1}H−^{1}H correlations to each other (~50:50 integration between both peaks), suggesting that they arise from chemically distinct static isomers in solution (for full COSY spectrum and expansions, see Figures S13 and S14).

temperature for D_2O), full coalescence could not be achieved with either complex, but significant broadening from fluxional isomerization could be clearly observed in both samples (Figures 6 and 7). The ^{1}H NMR of [Lu(C3octapa)]$^{-}$ demonstrated broad signals at ambient temperature (Figure 6), suggesting fluxional isomerization (slow on the NMR time scale). As the temperature was increased to 85 °C in 20 °C increments, the peaks were observed to coalesce, merging toward 4 broad alkyl-region peaks (Figure 6) as the rate of fluxional interconversion increased, correlating to the 4 unique ^{1}H NMR signals observed as singlets in the spectra of the free ligand H_4C3octapa (Figure 1). [In(C3octapa)]$^{-}$ showed sharp but complicated ^{1}H NMR splitting patterns at ambient temperature, suggesting the presence of multiple static isomers, with peaks broadening and beginning to coalesce as the temperature was increased to 85 °C (Figure 7). At 85 °C, the ^{1}H NMR signals of [In(C3octapa)]$^{-}$ also appeared to be coalescing toward 4 broad signals in a manner similar to that observed with [Lu(C3octapa)]$^{-}$; however, the signals from [Lu(C3octapa)]$^{-}$ remained substantially broader (Figure 6) than those observed for the In^{3+} complex (Figure 7), suggesting a higher energetic barrier to fluxional interconversion for [In(C3octapa)]$^{-}$. It can also be observed that the signals arising from the central propylene bridge $-CH_2-$ group of [In(C3octapa)]$^{-}$ (red arrow, Figure 3) began to merge at elevated temperatures (Figure 7), further supporting the assignment of these two signals as arising from different isomers, where coalescence from signal averaging began to occur at faster rates of fluxional interconversion at higher temperatures. At higher temperatures (e.g., 135 °C in DMSO-d_6), a further increase in coalescence would be expected for both samples; however, D_2O was chosen as solvent for its biological relevance.

Fluxional complexes of radiometals may ultimately be unfavorable. The rapid process of metal ion deligation−ligation by ligand donor arms, which can occur as the fluxional complex constantly rearranges and shifts between isomers in solution, could open temporary holes in the coordination sphere. When these holes in the coordination sphere occur in vivo, they may provide competing ligands such as aqua, phosphate, and serum proteins (e.g., transferrin or serum albumin) opportunities to bind to the metal ion and facilitate transchelation/demetalation. Furthermore, the presence of a well-defined, single static metal−ligand isomer (as in [In(octapa)]$^{-}$) of an acyclic metal complex would be ideal. Even having multiple static isomers of a metal−ligand complex in solution is not ideal because, due to their different structures, they may exhibit different physical properties and susceptibilities to external ligand attack. If this were the case, then these different static isomers may effectively exhibit different kinetic off-rates and therefore different in vivo stability and kinetic inertness. It is important to note that this discussion pertains to isomers formed during metal coordination by a ligand and not isomers of the ligand itself. The case of ligand isomerization is demonstrated by CHX-DTPA (Chart 1), which has 4 isomers (two pairs of diastereomers, CHX-A′-DTPA, CHX-A″-DTPA, CHX-B′-DTPA, CHX-B″-DTPA), and it was observed that the single CHX-A″-DTPA isomer was substantially more stable than the other 3 isomers.[23,24,54,55] The idea of correlating the degree of metal−ligand fluxional

dx.doi.org/10.1021/ic501466z | Inorg. Chem. 2014, 53, 10412−10431

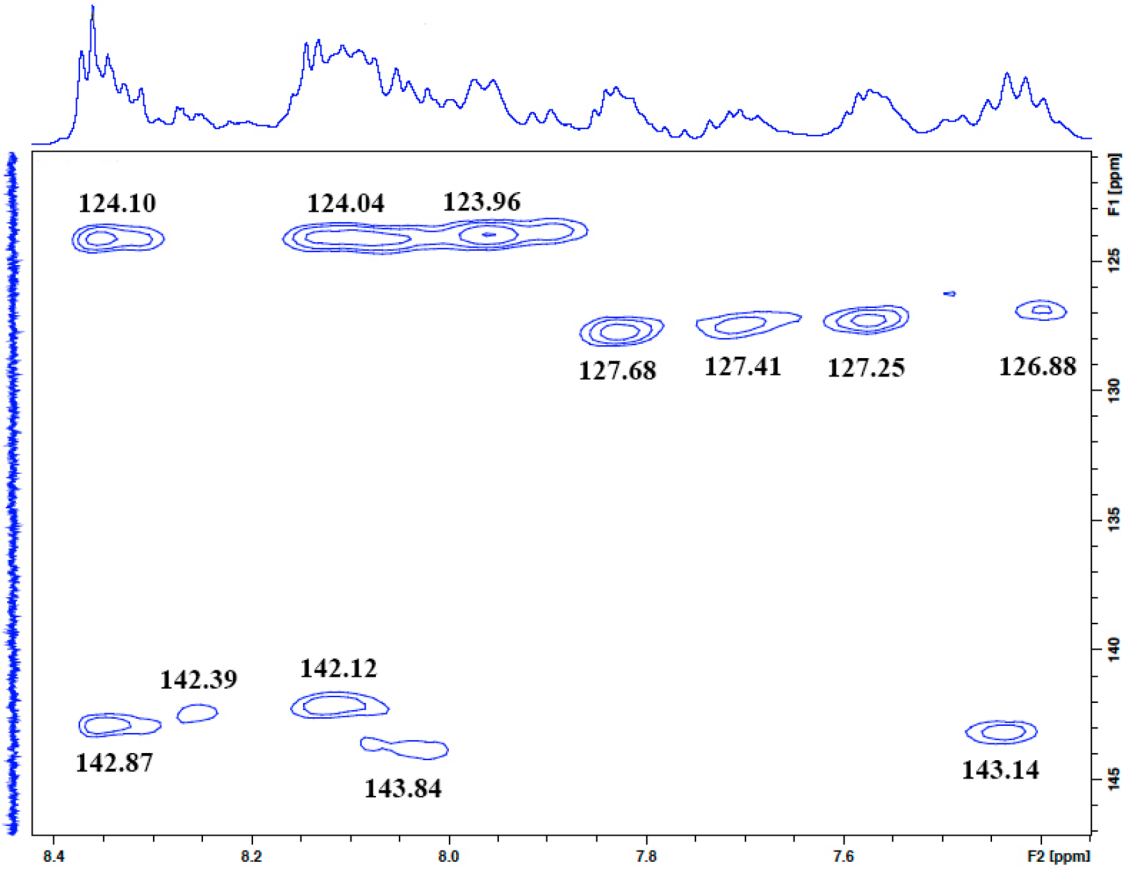

Figure 4. $^{1}H-^{13}C$ HSQC NMR (400/100 mHz, D_2O, 25 °C) expansion of aromatic signals in the spectrum of $[In(C3octapa)]^-$, showing correlations to 12 unique ^{13}C signals, with an additional aromatic signal at 125.32 ppm not shown (13 aromatic carbon atoms total) (^{13}C NMR spectra externally referenced to MeOH in D_2O) (for full HSQC spectrum and expansions, see Figures S17 and S18).

isomerization to in vivo stability is not established. However, the increased fluxionality and number of isomers observed here for H_4C3octapa complexes compared to the analogous H_4octapa complexes does appear to correlate to substantially inferior radiolabeling and serum stability properties for H_4C3octapa (vide infra). This concept may be valid only for acyclic ligands and therefore may not translate to macrocyclic complexes. For example, $[In(DOTA)]^-$ has been observed to be fluxional at ambient temperature through ^{1}H NMR experiments but is remarkably stable and kinetically inert in vivo.[56,57] The rapid interconversion between isomers of a macrocyclic metal ion complex like $[In(DOTA)]^-$ may not provide the same holes in the coordination sphere for competing ligands to access the metal center, as the metal ion remains enshrouded and protected within the macrocyclic framework during this process, making transchelation slower and less likely to occur. A thorough investigation comparing the level of fluxionality of acyclic metal complexes to their radiolabeling and stability properties would be required, which, to our knowledge, has not been adequately performed.

Acid Dissociation Constants. The pK_a values of ligand donor groups can effect metal coordination and radiolabeling properties, and to further study this, we experimentally determined the acid dissociation constants (pK_a) for H_4C3octapa by potentiometric titrations. For example, a lower pK_a value for functional groups such as phenols and carboxylic acids means that those acidic protons are more easily removed (at lower pH values), which allows for metal coordination and radiolabeling at lower pH values. A difference in pK_a values can be observed when comparing H_4C3octapa to H_4octapa. Table 1 shows the acid dissociation constants for both H_4C3octapa and H_4octapa, with the HL and H_2L equilibrium quotients corresponding to the protonation of backbone nitrogen atoms (1,3-propylenediamine and 1,2-ethylenediamine, respectively). Although chemically identical, these two nitrogen atoms have significantly different pK_a values, as a result of charge repulsion when the two nitrogen atoms are protonated in the H_2L species. For H_4octapa, the difference in pK_a is 3 units between these two protonated nitrogen atoms, with the deprotonation of the first backbone-en nitrogen occurring with a pK_a of 5.59(6) (H_2L), and the second, with a pK_a of 8.59(4) (HL). The explanation for this is that the two positively charged protonated nitrogen atoms (H_2L) of the 1,2-ethylenediamine backbone of H_4octapa are held physically close together through the ethylene bridge, creating substantial charge repulsion between them, therefore making the first deprotonation event from H_2L to HL more favorable and more acidic with a lower pK_a (5.59(6) vs 8.59(4)). The effect of extending the two-carbon ethylene (en) bridge of H_4octapa to a three-carbon propylene (pn) bridge for the H_4C3octapa derivative is that this charge repulsion is decreased, therefore reducing the thermodynamic driving force for removal of the first H_2L proton. The effect of this is that the pK_a for removal of the first H_2L 1,3-propylenediamine nitrogen proton in H_4C3octapa is over 1 unit higher (more basic) than that for H_4octapa, with values of 6.95(6) for H_2L and 8.86(3) for HL (Table 1). Table 1 also contains pK_a values for the picolinic acid groups (H_4L and H_3L) and the carboxylic acid arms (H_6L

dx.doi.org/10.1021/ic501466z | Inorg. Chem. 2014, 53, 10412−10431

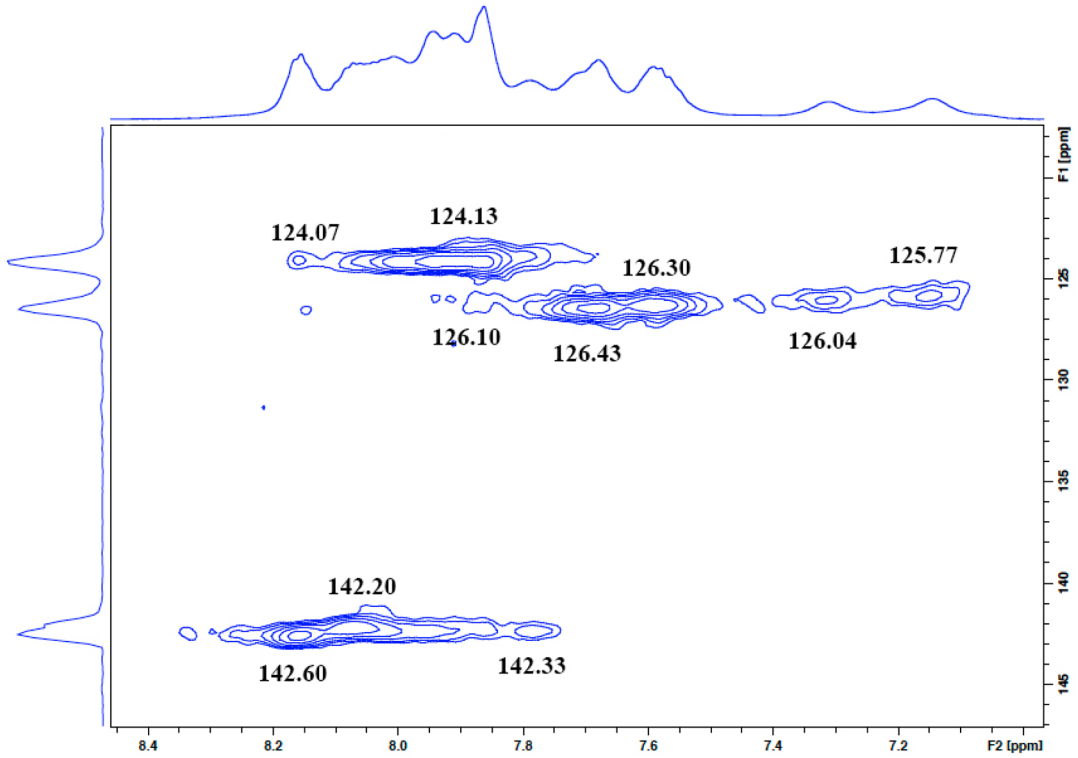

Figure 5. $^{1}H-^{13}C$ HSQC NMR (600/150 mHz, D_2O, 25 °C) expansion of aromatic signals in spectrum of $[Lu(C3octapa)]^-$, showing correlations to 10 unique ^{13}C signals, with spectral resolution being worse than that of $[In(C3octapa)]^-$ in Figure 4 due to the broad signals from fluxional isomerization (^{13}C NMR spectra externally referenced to MeOH in D_2O) (for full HSQC spectrum and expansions, see Figures S19 and S20).

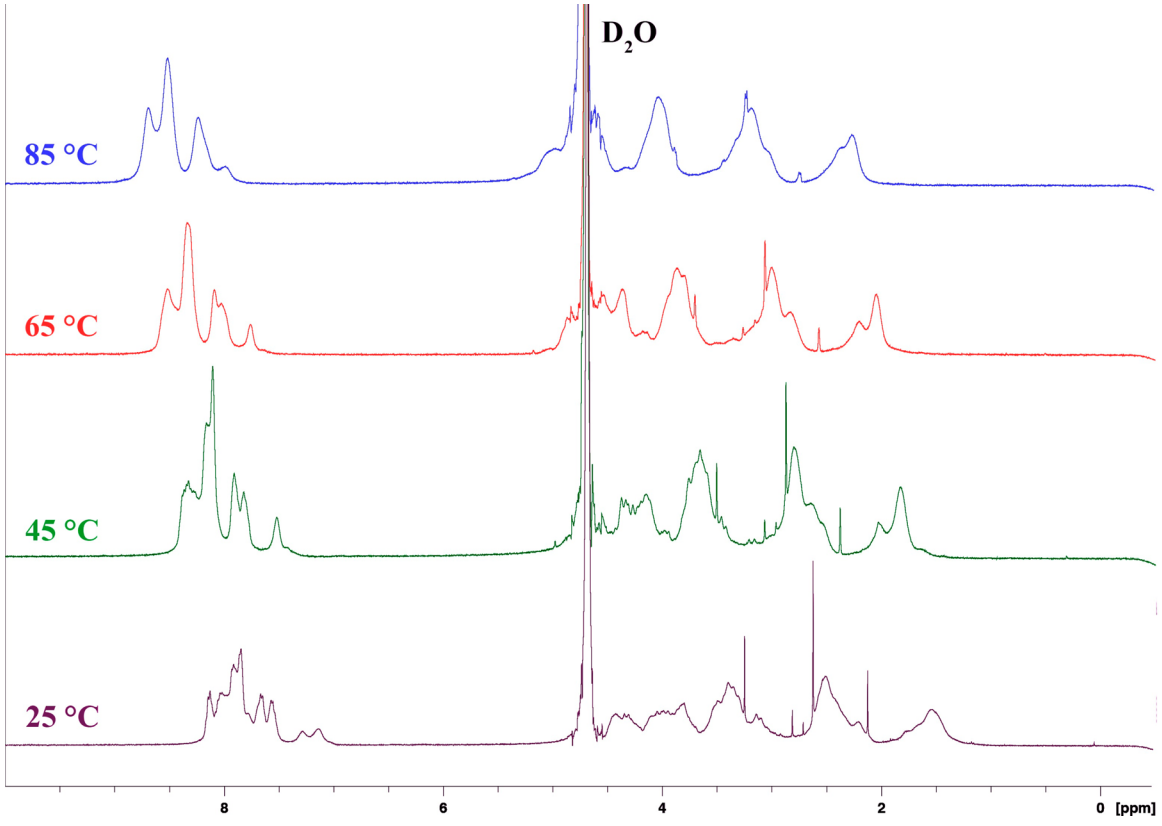

Figure 6. Variable temperature (VT) NMR experiments with $[Lu(C3octapa)]^-$ (D_2O, 400 MHz), showing broad signals at 25 °C most likely arising from fluxional isomers and/or aqua ligand exchange at 25 °C, with further broadening and coalescing being observed as the temperature was increased to 85 °C in 20 °C increments, suggesting fluxional isomerization between multiple isomers was increased elevated temperatures.

dx.doi.org/10.1021/ic501466z | Inorg. Chem. 2014, 53, 10412−10431

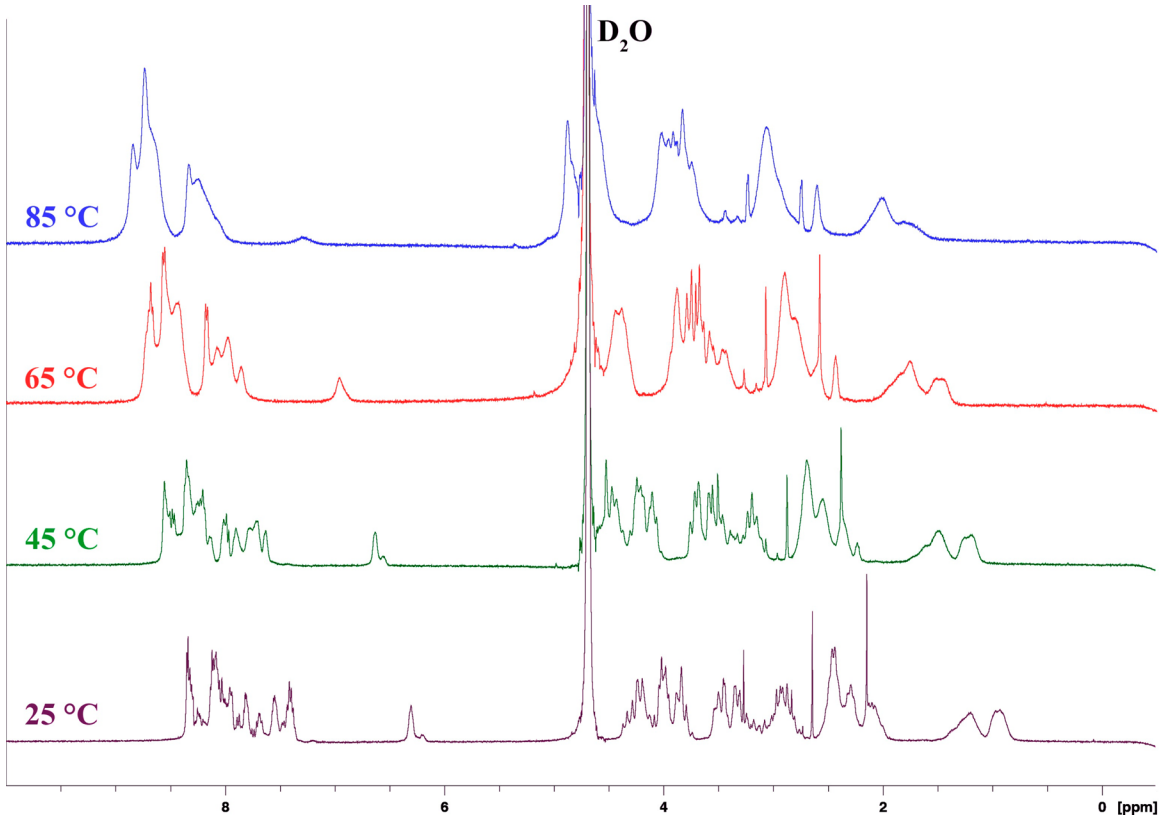

Figure 7. Variable temperature (VT) NMR experiments with $[In(C3octapa)]^-$ (D_2O, 400 MHz), showing sharp signals and coupling patterns most likely arising from multiple static isomers at 25 °C, broadening and coalescing as the temperature was increased to 85 °C in 20 °C increments, suggesting fluxional isomerization between multiple isomers at elevated temperatures.

Table 1. Acid Dissociation Constants (pK_a), Formation Constants (log K_{ML}), and pM[a] Values for In^{3+} and Lu^{3+} Complexes of H_4octapa and H_4C3octapa

	log K	
equilibrium quotient	H_4C3octapa, C3octapa^{4-} = L	H_4octapa, octapa^{4-} = L
$[H_6L]/[H_5L][H]$	N/D	N/D
$[H_5L]/[H_4L][H]$	2.0(1)	2.79(4)
$[H_4L]/[H_3L][H]$	2.65(8)	2.77(4)
$[H_3L]/[H_2L][H]$	3.54(7)	3.77(2)
$[H_2L]/[HL][H]$	6.95(6)	5.59(6)
$[HL]/[H][L]$	8.86(3)	8.59(4)
$[InL]/[In][L]$	24.6(3)	26.76(14)
$[InHL]/[InL][H]$	N/D	2.89(23)
pM[a]	24.0	26.5
$[LuL]/[Lu][L]$	18.8(3)	20.08(9)
pM[a]	18.1	19.8

[a]Calculated for 10 μM total ligand and 1 μM total metal at pH 7.4 and 25 °C.

and H_5L). The pK_a value for the first deprotonation event of the H_6L carboxylic acid could not be determined, as the value was below the threshold of the electrode (pH < 2).

Thermodynamic Stability. In order to indirectly test the hypothesis that decreased fluxional isomerization may correlate to increased stability (with acyclic ligands), we have evaluated the thermodynamic stability of the In^{3+} and Lu^{3+} metal complexes of H_4C3octapa using potentiometric titrations to determine their formation constants. The molecular formula of H_4C3octapa was determined by elemental analysis (H_4C3octapa·4HCl·2H_2O), and thermodynamic formation constants for H_4octapa were previously studied.[14,28] The thermodynamic stability constants (log K_{ML}) for H_4C3octapa with In^{3+} and Lu^{3+} were determined by competitive potentiometric titration experiments with EDTA, under the same experimental conditions as those previously used for H_4octapa.[14,28] The thermodynamic stability constants (log K_{ML}) for In^{3+} and Lu^{3+} with H_4C3octapa were experimentally determined to be 24.6 ± 0.3 (pM = 24.0) and 18.8 ± 0.3 (pM = 18.1), respectively (Table 2). The thermodynamic stability

Table 2. Formation Constants (log K_{ML}) and pM[a] Values for In^{3+}, Lu^{3+}, and Y^{3+} Complexes of Relevant Ligands

ligand	metal ion	log K_{ML}	pM[a]	ref
dedpa^{2-}	In^{3+}	26.60(4)	25.9	14
octapa^{4-}	In^{3+}	26.8(1)	26.5	14
	Lu^{3+}	20.08(9)	19.8	28
C3octapa^{4-}	In^{3+}	24.6(3)	24.0	
	Lu^{3+}	18.8(3)	18.1	
DTPA^{4-}	In^{3+}	29.0	25.7	65 and 66
	Lu^{3+}	22.6	19.1	28 and 66
DOTA^{4-}	In^{3+}	23.9(1)	18.8	61 and 66
	Lu^{3+}	21.6(1), 23.6, 25, 29.2	17.1	28 and 58−60
transferrin	In^{3+}	18.3	18.7	67
	Lu^{3+}	11.08		68

[a]Calculated for 10 μM total ligand and 1 μM total metal at pH 7.4 and 25 °C.

dx.doi.org/10.1021/ic501466z | Inorg. Chem. 2014, 53, 10412−10431

constants of the In^{3+} complexes of H_4octapa, DOTA, and DTPA have been previously determined to be 26.6 (pM = 26.5), 23.9 (pM = 18.8), and 29.0 (pM = 25.7), respectively (Table 2).[14] The thermodynamic stability constants of the Lu^{3+} complexes of H_4octapa, DOTA, and DTPA have been previously determined to be 20.08 (pM = 19.8), 21.6−29.2 (pM = 17.1), and 22.6 (pM = 19.1), respectively (Table 2).[28] The reason for the large variance in DOTA-Lu^{3+} stability constants is that many different methods have been used due to the very slow kinetics of DOTA for forming metal ion complexes.[28,58−60] The pM value is a condition-dependent value that is calculated from the standard thermodynamic stability constant (log K_{ML}), accounting for variables and conditions such as ligand basicity (pK_a), metal ion hydrolysis, pH (physiological, 7.4), and a set ligand/metal ratio (10:1). The pM (= −log[M]) is essentially the metal scavenging ability of the ligand under biologically relevant conditions; the higher the pM value, the lower the concentration of free metal ion.[61−64] These experimentally determined values show that H_4C3octapa forms less thermodynamically stable complexes with In^{3+} and Lu^{3+} than does the ligand H_4octapa. The log K_{ML} and pM values were determined to be ∼2 units lower (∼2 orders of magnitude difference in thermodynamic stability) for H_4C3octapa than for H_4octapa with both In^{3+} and Lu^{3+}. These lower log K_{ML} and pM values are consistent with H_4C3octapa being a worse fit than H_4octapa for these large metal ions, with DFT calculations predicting lower symmetry and less ideal bond lengths/angles (see DFT section), and NMR studies showing higher levels of isomerization and fluxional interconversion. The lower thermodynamic stability of H_4C3octapa with these metal ions also correlates to inferior radiolabeling and serum stability properties with ^{111}In and ^{177}Lu (vide infra).

Although thermodynamic stability is generally regarded as an unreliable predictor of in vivo stability on its own[69] and the kinetic inertness of a radiometal complex is a much more relevant factor, we hope to observe trends by comparing NMR, DFT, thermodynamic, and in vitro/in vivo stability data. A common example of this is the case of $[^{111}In(DOTA)]^-$, where it is widely accepted as being significantly more stable than $[^{111}In(DTPA)]^{2-}$ both in vivo and in vitro; however, the thermodynamic stability constant for DTPA with In^{3+} is ∼5 units higher (∼5 orders of magnitude difference in thermodynamic stability) than that for DOTA (29.0 and 23.9, respectively) (Table 1). Comparing the thermodynamic stability and the in vivo stability of DTPA and DOTA like this may appear to be a compelling example of why thermodynamic stability values are not reliable predictors of in vivo stability; however, as mentioned above, it may be that comparing acyclic ligands to macrocyclic ligands is not possible by these methods, and perhaps trends within each class of ligand, acyclic and macrocyclic, may emerge in the future as more data are collected. It appears that in this work the lower thermodynamic stability of H_4C3octapa (∼2 orders of magnitude) compared to that of H_4octapa does indeed correlate to lower in vitro stability in radiolabeling experiments (vide infra) and presumably lower in vivo stability.

Density Functional Theory Structure Calculations. Growing crystals of the metal complexes discussed herein for solid-state X-ray analysis proved to be difficult, so density functional theory (DFT) calculations were performed. The coordination geometries of 8-coordinate $[In(C3octapa)]^-$ and $[Lu(C3octapa)]^-$ were calculated in silico using DFT methods to compare their geometries, polar surface areas, and bond lengths/angles (Figure 8). The DFT structures of the 8-coordinate $[In(octapa)]^-$ and $[Lu(octapa)]^-$ complexes were calculated previously, and MEP polar surface area maps were superimposed onto the structures.[14,28] A visual inspection of In^{3+} and Lu^{3+} complexes of both ligands suggests they are very similar to one another, with similar charge distributions determined by the overlaid molecular electrostatic potential (MEP) polar surface area maps (Figure 8).[14,28]

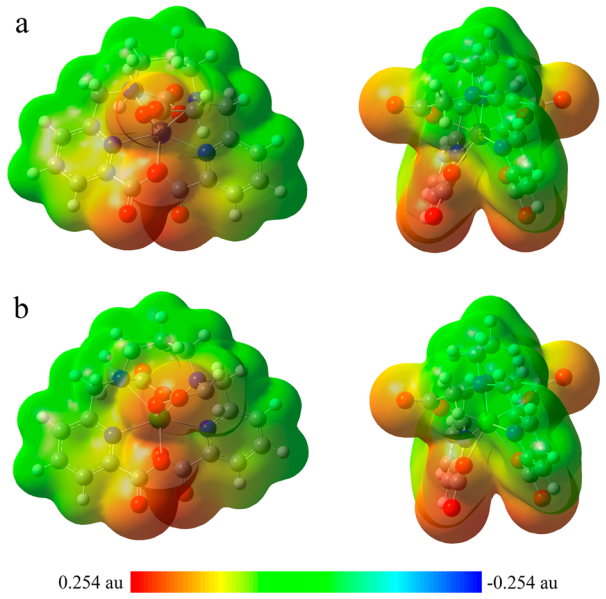

Figure 8. In silico DFT structure predictions: (a) 8-coordinate structure of $[In(C3octapa)]^-$ (top) from two perspectives; (b) 8-coordinate structure of $[Lu(C3octapa)]^-$ (bottom) from two perspectives, with both structures showing overlaid MEP polar-surface area maps predicting the charge distribution over the solvent-exposed surface of the metal complexes (red = negative, blue = positive, representing a maximum potential of 0.254 au and a minimum of −0.254 au, mapped onto electron density isosurfaces of 0.002 $Å^{-3}$). Performed using the B3LYP functional employing the 6-31+G(d,p) basis set for first- and second-row elements, and the Stuttgart/Dresden and associated ECP's basis set was employed for the metals, lutetium and indium.[40,41] Solvent (water) effects were described through a continuum approach by means of the IEF PCM as implemented in Gaussian 09.

Upon qualitative visual comparison, the structures and charge distributions are very similar between these $[C3octapa]^-$ complexes and the $[In(octapa)]^-$ and $[Lu(octapa)]^-$ DFT structures, but a deeper analysis of bond lengths and angles reveals a more interesting comparison.[14,28] It has been proposed by Hancock that the ideal L−M−L bond angle and ideal M−L bond length for a 6-membered L−M−L chelate ring (e.g., 1,3-propylenediamine) is 109.5° and 1.6 Å, respectively, and for a 5-membered chelate ring (e.g., 1,2-ethylenediamine), 69° and 2.5 Å, respectively, with 5-membered chelate rings being ideal for larger metal ions (e.g., In^{3+} and Lu^{3+}) and 6-membered chelate rings being ideal for a small metal (the approximate size of a sp^3-hybridized carbon).[11] These predictions are not concrete but will be compared to the DFT calculated values for H_4octapa and H_4C3octapa metal complexes. A selection of bond lengths and angles from DFT calculated ML complexes are shown in Table 3.

The bond lengths for the H_4C3octapa complexes diverge from the optimum M−L values proposed by Hancock of 1.6 Å

dx.doi.org/10.1021/ic501466z | Inorg. Chem. 2014, 53, 10412−10431

Table 3. Relevant Bond Lengths (Å) and Angles (deg) Comparing the DFT-Calculated In^{3+} and Lu^{3+} Complexes of H_4octapa and H_4C3octapa

bond lengths (Å)	[In(octapa)]$^-$	[In(C3octapa)]$^-$	[Lu(octapa)]$^-$	[(Lu(C3octapa)]$^-$
(Ac-COO) O1−M	2.200	2.213	2.218	2.296
(Ac-COO) O2−M	2.201	2.250	2.218	2.280
(pyr-COO) O3−M	2.295	2.263	2.315	2.326
(pyr-COO) O4−M	2.294	2.280	2.315	2.325
(en/pn-N) N1−M	2.538	2.494	2.756	2.593
(en/pn-N) N2−M	2.538	2.486	2.756	2.576
(pyr-N) N3−M	2.241	2.256	2.501	2.451
(pyr-N) N4−M	2.241	2.280	2.501	2.399
N1−M−N2 angle (deg)	74.8	93.0	67.8	90.8

for a 6-membered chelate ring, with bond lengths calculated of 2.494/2.486 Å for the In^{3+} complex and 2.593/2.576 Å for the Lu^{3+} complex (Table 3). The 1,2-ethylenediamine M−L bond lengths of the H_4octapa complexes were close to the reported ideal lengths of 2.5 Å, with values being calculated to be 2.538/2.538 Å for the In^{3+} complex and 2.756/2.756 Å for the Lu^{3+} complex (Table 3). For the H_4C3octapa complexes, the numbers obtained for the 1,3-propylenediamine L−M−L bond angles deviated more significantly from the proposed optimal L−M−L angle of 109.5°, with calculated values of 93.0 and 90.8° for In^{3+} and Lu^{3+}, respectively (Table 3). For the H_4octapa complexes, on the other hand, the ethylene N1−M−N2 bond angle was calculated to be closer to the proposed ideal angle of 69°, with values of 74.8 and 67.8° for In^{3+} and Lu^{3+}, respectively. An inspection of the bond lengths presented in Table 3 highlights the very symmetric nature of M−L bonds in the H_4octapa complexes ($\sim C_2$ symmetry) and the comparatively asymmetric bonds for the H_4C3octapa complexes, which supports the NMR data (vide supra). The NMR spectra of the H_4C3octapa complexes revealed lower symmetry and more fluxional species than the H_4octapa complexes, mirroring the data from DFT-calculated structures (Table 3). These results suggest that the H_4octapa complexes should be more stable and inert than the analogous H_4C3octapa complexes. Although it is interesting to compare these DFT-calculated bond lengths and angles to the ideal values proposed by Hancock, evaluating the stability of the radiometal complexes is perhaps more relevant.

Trastuzumab Antibody Conjugation, ^{111}In/^{177}Lu Radiolabeling, and In Vitro Serum Stability. To gain further insight into their differences in stability (thermodynamic and kinetic), we conjugated the bifunctional ligand derivatives *p*-SCN-Bn-H_4C3octapa and *p*-SCN-Bn-H_4octapa to the antibody trastuzumab, radiolabeled the resulting ligand−antibody immunoconjugate with ^{111}In and ^{177}Lu, and evaluated their stability via their inertness to transchelation by serum proteins over a period of 5 days (vide infra). As discussed in the introduction, the boundary between large and small metal ions for the most stable fit between 5- and 6-membered chelate rings is unclear. These radiolabeling and serum stability studies aim to make this boundary clear for the radiometals ^{111}In and ^{177}Lu. NMR studies, thermodynamic formation constants, and DFT structure analysis have suggested that H_4octapa is a superior ligand to H_4C3octapa for the large metal ions In^{3+} and Lu^{3+}, and that the addition of a single carbon to the structure of H_4C3octapa was detrimental. Ultimately, the stability and inertness of these metal ion complexes must be evaluated in vitro and in vivo. Radiometric isotopic dilution assays for determining the number of chelates bound to each antibody were not performed, as previous experiments with *p*-SCN-Bn-H_4octapa and *p*-SCN-Bn-DOTA found that the addition of 4 equiv. of isothiocyanate-ligand to trastuzumab would reliably conjugate ∼3 chelates per antibody.[28] Further to this point, the purpose of this study is to determine the difference in stability between ligands, and a difference of a few chelates per antibody would have a negligible, if any, effect on serum stability and dissociation rates. For studies trying to determine the maximum specific activity achievable for each ligand−antibody conjugate, however, the number of chelates per antibody would be a crucial piece of data.

To evaluate and compare the stability of these ligands in biologically relevant media, the nonbifunctional ligands H_4octapa and H_4C3octapa, along with gold standard ligands DOTA and DTPA were radiolabeled with ^{177}Lu and incubated in human blood serum as a transchelation challenge. The amount of ^{177}Lu transchelated from ligands to serum proteins was measured at 1.5 and 24 h using PD10 size-exclusion columns. The results summarized in Table 2 reveal that the stability of H_4octapa, H_4C3octapa, and DOTA in human serum was nearly identical during a 24 h period, with DTPA having slightly lower stability. These results are observed to diverge from the serum stability values obtained for the same ligands but as bifunctional derivatives conjugated to the antibody trastuzumab (vide infra).

Table 4. Human Serum Stability Challenge[a]

complex	1.5 h stability (%)	24 h stability (%)
[^{177}Lu(C3octapa)]$^-$	90.3 ± 1.8	86.2 ± 1.0
[^{177}Lu(octapa)]$^-$	88.1 ± 1.2	87.7 ± 0.7
[^{177}Lu(DOTA)]$^-$	87.7 ± 0.7	87.4 ± 2.1
[^{177}Lu(DTPA)]$^{2-}$	77.4 ± 1.2	81.6 ± 2.3

[a]Performed at 37.5 °C (n = 3), with stability shown as the percent intact ^{177}Lu complex, determined by PD10 size-exclusion column elution.

Although the results summarized in Table 4 suggest that the ^{177}Lu complexes of H_4C3octapa and H_4octapa possess identical stability against serum transchelation, a much more relevant experiment is to evaluate their stability when attached to a targeting vector like trastuzumab. The practical difficulty with this approach is that bifunctional ligands are typically much more difficult to synthesize, so for early screening of new ligands, the nonbifunctional derivatives are often more expedient to use. Despite convenience, a more biologically relevant model system was evaluated by conjugating the bifunctional ligands to the HER2/*neu*-targeting antibody

dx.doi.org/10.1021/ic501466z | Inorg. Chem. 2014, 53, 10412−10431

trastuzumab. In order to provide a basis for comparison, immunoconjugates were synthesized bearing both *p*-SCN-Bn-H_4C3octapa and *p*-SCN-Bn-H_4octapa bifunctional chelates, they were radiolabeled, and serum stability experiments were performed. To begin, trastuzumab was purified by centrifuge filtration to remove additives present in the antibody kit (e.g., L-histidine HCl), mixed under basic conditions (pH 8.5–9.0) with 4 equiv of *p*-SCN-Bn-H_4C3octapa or *p*-SCN-Bn-H_4octapa to react, and finally purified via size-exclusion chromatography (PD-10, GE Healthcare, UK). H_4C3octapa–trastuzumab and H_4octapa–trastuzumab were then radiolabeled with either ^{111}In or ^{177}Lu in NH_4OAc buffer (pH 5.5, 200 mM) for 60 min at room temperature to ensure maximum radiolabel incorporation. H_4octapa–trastuzumab has been previously determined to radiolabel quantitatively with ^{111}In and ^{177}Lu in 15 min at ambient temperature;[28] results that were reproduced here with >95% radiochemical yields for both ^{111}In and ^{177}Lu with high radiochemical purity (>99% in each case) and specific activity (~2.2 and ~2.5 mCi/mg, respectively, iTLC traces in Figures S21 and S22). H_4C3octapa–trastuzumab radiolabeled with ^{111}In and ^{177}Lu in radiochemical yields and specific activities of ~95% (~2.3 mCi/mg) and ~8% (~0.3 mCi/mg), respectively (iTLC traces in Figures S23 and S24). It was observed that a substantial amount of ^{177}Lu was eluted by the EDTA-containing iTLC mobile phase upon analysis of radiolabeling yields for ^{177}Lu-C3octapa–trastuzumab, suggesting facile transchelation of ^{177}Lu by EDTA and therefore very low stability of the H_4C3octapa complex.

In order to assay the stability of these radioimmunoconjugates under biologically relevant conditions, all four radiolabeled constructs were incubated in human serum and PBS (control) at 37 °C for a period of 5 days (Figures 9 and 10). At

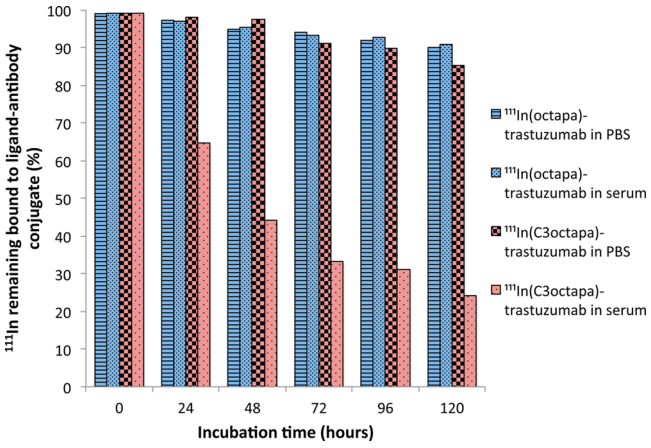

Figure 9. Stability of the immunoconjugates ^{111}In(octapa)–trastuzumab and ^{111}In(C3octapa)–trastuzumab in both phosphate buffered saline (PBS) and human blood serum, evaluated by spotting ~1 μCi of serum competition mixture on silica-embedded paper iTLC strips and eluting with an aqueous EDTA (50 mM, pH 5) mobile phase.

the end of 5 days, the stability of the ^{111}In-C3octapa– and ^{111}In-octapa–trastuzumab immunoconjugates was determined to be ~24 and ~91%, respectively, revealing a significant decrease in stability of the radiometal complexes of H_4C3octapa compared to that of H_4octapa (Figure 9). The ^{177}Lu-C3octapa– and ^{177}Lu-octapa–trastuzumab conjugates were found to be ~4 and ~89% stable after 5 days, respectively,

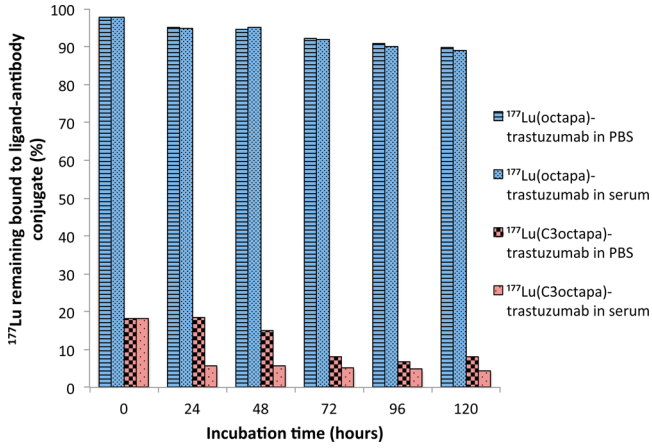

Figure 10. Stability of the immunoconjugates ^{177}Lu(octapa)–trastuzumab and ^{177}Lu(C3octapa)–trastuzumab in both phosphate buffered saline (PBS) and human blood serum, evaluated by spotting ~1 μCi of serum competition mixture on silica-embedded paper iTLC strips and eluting with an aqueous EDTA (50 mM, pH 5) mobile phase.

showing a more drastic decrease in stability than that observed for the analogous ^{111}In complexes (Figure 10). Although it was known that 6-membered ligand–metal chelate rings (as with H_4C3octapa) are less favorable than 5-membered chelate rings for large metal ions (as with H_4octapa),[11] these serum stability results prove this point more dramatically than expected.

During elution of the iTLC strips, the ligand EDTA is present in great excess (50 mM) over the small amount of radioimmunoconjugate spotted onto the iTLC strips (0.5–1 μL of serum competition mixture) and therefore transchelation during elution is possible (Figures S21–S24). The four serum stability challenges were therefore run in both human serum and phosphate buffered saline (PBS) as a control to determine if transchelation and radiometal leaching was occurring as a result of serum proteins or because of the excess of EDTA present in the iTLC mobile phase (Figures 9 and 10). For the ^{111}In/^{177}Lu-octapa–trastuzumab samples, there was <1% difference in stability between serum and PBS solutions. The H_4C3octapa samples demonstrated more interesting results, with the stability of ^{111}In-C3octapa–trastuzumab after 120 h in serum being ~24%, but this was much higher, at ~85%, in PBS (Figure 9). This result reveals that in a solution of PBS the ^{111}In-C3octapa–trastuzumab immunoconjugate remains stable and that very little ^{111}In is transchelated by EDTA during iTLC elution, but when placed in a solution of blood serum, a substantial amount of ^{111}In was transchelated by serum proteins.

The stability of ^{177}Lu-C3octapa–trastuzumab after 5 days in PBS and serum was ~8 and ~4%, respectively, suggesting that the $[^{177}$Lu(C3octapa)$]^-$ complex is very unstable, being easily transchelated by PBS and/or the EDTA present in the iTLC mobile phase (Figure 10). One of the reasons for the poor radiolabeling yield and specific activity of H_4C3octapa–trastuzumab with ^{177}Lu was that the complex formed was very weak, with initial iTLC analyses after radiolabeling showing substantial leaching of ^{177}Lu from the immunoconjugate to the EDTA mobile phase (Figures S21–S24).

The difference of a single carbon in the backbone of this ligand scaffold clearly results in a substantial decrease in stability with these radiometals. The denticity and binding

dx.doi.org/10.1021/ic501466z | Inorg. Chem. 2014, 53, 10412–10431

groups were not changed between H_4octapa and H_4C3octapa, demonstrating the crucial importance of chelate ring size and ligand−metal bite size/angle, reinforcing the importance of carefully matching bifunctional chelators with radiometals for imaging and therapeutic applications.[8] These results also suggest that evaluating the stability of nonbifunctional ligands with serum transchelation experiments, using PD10 size-exclusion elution as a method of analysis, may not be a reliable method. It was found that the nonbifunctional $[^{177}$Lu(C3octapa)$]^-$ complex was very stable to serum transchelation by PD10 size-exclusion analysis but was very unstable as the bifunctional trastuzumab conjugate by iTLC analysis. This mirrors previous results where the radiometal complex $[^{111}$In(decapa)$]^{2-}$ was found to be stable by PD10 size-exclusion analysis, but in vivo biodistribution results suggested that it was not stable. These results suggest that in vitro serum stability analysis of nonbifunctional ligands should be investigated with a more rigorous technique like size-exclusion HPLC. It may also be the case that only experiments with bifunctional ligand derivatives should be undertaken, as the nonbifunctional ligands will generally not be used for radiopharmaceutical applications and only bifunctional chelate conjugates are of utility. The difficulty of synthesizing most bifunctional ligands could, however, make this approach time consuming and inefficient.

CONCLUSIONS

The ligands H_4C3octapa and *p*-SCN-Bn-H_4C3octapa were synthesized for the first time, using nosyl protection chemistry, for comparison to the previously studied ligands H_4octapa and *p*-SCN-Bn-H_4octapa. The purpose of this work was to determine whether addition of a single carbon atom to the backbone of these ligand scaffolds would effect metal/radiometal chelation and stability. The In^{3+} and Lu^{3+} complexes of H_4C3octapa were synthesized, studied by NMR spectroscopy, DFT structure analysis, and potentiometric titrations, and compared to the analogous H_4octapa complexes. It was found that the ^{1}H NMR spectra of $[$In(C3octapa)$]^-$ and $[$Lu(C3octapa)$]^-$ were substantially different from the analogous H_4octapa complexes, with fluxional isomerization and a higher number of isomers being observed by VT-NMR and 2D COSY/HSQC-NMR experiments. Evaluation of DFT structures revealed very symmetric $[$In(octapa)$]^-$ and $[$Lu(octapa)$]^-$ complexes, with a 5-member chelate ring being formed between the *N*,*N*′-ethylene backbone and the metal centers yielding very symmetric structures. In contrast, the $[$In(C3octapa)$]^-$ and $[$Lu(C3octapa)$]^-$ complexes were much less symmetric, with a 6-membered chelate ring being formed between the *N*,*N*′-propylene backbone and the metal centers, supporting the NMR spectral analysis that these complexes are less symmetric and rigid than the analogous H_4octapa complexes. Potentiometric titrations were performed to determine the formation constants (log K_{ML}, pM), which found the thermodynamic stability to be ∼2 orders of magnitude lower for the In^{3+} and Lu^{3+} complexes of H_4C3octapa when compared to that of the analogous complexes of the H_4octapa ligand. The bifunctional ligands *p*-SCN-Bn-H_4C3octapa and *p*-SCN-Bn-H_4octapa were conjugated to the HER2/*neu* targeting antibody trastuzumab and radiolabeled with ^{111}In and ^{177}Lu, and their radiochemical yields and serum stability were directly compared. It was observed that the H_4C3octapa−trastuzumab conjugates displayed inferior radiochemistry properties to that of H_4octapa−trastuzumab, with radiochemical yields and serum stability being substantially worse. Over a 5 day stability challenge experiment in blood serum, ^{111}In-octapa− and ^{111}In-C3octapa−trastuzumab immunoconjugates were determined to be ∼91 and ∼24% stable, respectively, and ^{177}Lu-octapa− and ^{177}Lu-C3octapa−trastuzumab, ∼89 and ∼4% stable, respectively. Although only a single carbon atom was added to H_4C3octapa and the metal donor atoms and denticity were not changed, the solution chemistry and radiochemistry properties were drastically altered, highlighting the importance of careful ligand design and radiometal−ligand matching when selecting a bifunctional chelator to conjugate to targeting vectors for radiopharmaceutical applications. The exact boundary between what is considered to be small and large metal ion radii for 5/6-membered chelate ring preference is still unclear. This work further suggests that large metal ions such as In^{3+} and Lu^{3+} form the most stable complexes when chelated by 5-membered chelate rings.

ASSOCIATED CONTENT

Supporting Information

^{1}H/^{13}C NMR spectra and select FT-ATR-IR spectra of final synthesized compounds. This material is available free of charge via the Internet at http://pubs.acs.org.

AUTHOR INFORMATION

Corresponding Authors

*(J.S.L.) Tel.: (646) 888-3038. Fax: (310) 206-8975. E-mail: lewisj2@mskcc.org.

*(M.J.A.) Tel.: (604) 222-7527. Fax: (604) 222-1074. E-mail: adam@triumf.ca.

*(C.O.) Tel.: (604) 822-4449. Fax: (604) 822-2847. E-mail: orvig@chem.ubc.ca.

Notes

The authors declare no competing financial interest.

ACKNOWLEDGMENTS

The authors thank Eszter Boros for initial assistance with ligand design. We acknowledge Nordion (Canada) and the Natural Sciences and Engineering Research Council (NSERC) of Canada for grant support (CR&D, Discovery), NSERC for CGS-M/CGS-D fellowships (E.W.P.), and the University of British Columbia for 4YF fellowships (E.W.P.). C.O. acknowledges the Canada Council for the Arts for a Killam Research Fellowship (2011-2013) and the University of Canterbury for a Visiting Erskine Fellowship (2013). Services provided by the MSKCC Small-Animal Imaging Core Facility were supported in part by NIH grants R24 CA83084 and P30 CA08748. The authors also thank the Department of Defense (award W81XWH-12-1-0029, B.M.Z.) and the DOE (award DE-SC0002184, J.S.L.) for their generous funding.

REFERENCES

(1) Rösch, F.; Baum, R. P. *Dalton Trans.* **2011**, *40*, 6104−6111.

(2) Zeglis, B. M.; Lewis, J. S. *Dalton Trans.* **2011**, *40*, 6168−6195.

(3) Wadas, T. J.; Wong, E. H.; Weisman, G. R.; Anderson, C. J. *Chem. Rev.* **2010**, *110*, 2858−2902.

(4) Deri, M. A.; Zeglis, B. M.; Francesconi, L. C.; Lewis, J. S. *Nucl. Med. Biol.* **2013**, *40*, 3−14.

(5) Zeglis, B. M.; Mohindra, P.; Weissmann, G. I.; Divilov, V.; Hilderbrand, S. A.; Weissleder, R.; Lewis, J. S. *Bioconjugate Chem.* **2011**, *22*, 2048−2059.

(6) Bartholomä, M. D.; Louie, A. S.; Valliant, J. F.; Zubieta, J. *Chem. Rev.* **2010**, *110*, 2903−2920.
(7) Ramogida, C. F.; Orvig, C. *Chem. Commun.* **2013**, *49*, 4720−4739.
(8) Price, E. W.; Orvig, C. *Chem. Soc. Rev.* **2014**, *43*, 260−290.
(9) Zeglis, B. M.; Houghton, J. L.; Evans, M. J.; Viola-Villegas, N.; Lewis, J. S. *Inorg. Chem.* **2014**, *53*, 1880−1899.
(10) Zeglis, B.; Holland, J.; Lebedev, A.; Cantorias, M.; Lewis, J., Radiopharmaceuticals for Imaging in Oncology with Special Emphasis on Positron-Emitting Agents. In *Nuclear Oncology*; Strauss, H. W., Mariani, G., Volterrani, D., Larson, S. M., Eds.; Springer: New York, 2013; pp 35−78.
(11) Hancock, R. D. *J. Chem. Educ.* **1992**, *69*, 615−621.
(12) Brechbiel, M. W. *Q. J. Nucl. Med. Mol. Imaging* **2008**, *52*, 166−173.
(13) Boswell, C. A.; Brechbiel, M. W. *Nucl. Med. Biol.* **2007**, *34*, 757−778.
(14) Price, E. W.; Cawthray, J. F.; Bailey, G. A.; Ferreira, C. L.; Boros, E.; Adam, M. J.; Orvig, C. *J. Am. Chem. Soc.* **2012**, *134*, 8670−8683.
(15) Boros, E.; Ferreira, C. L.; Cawthray, J. F.; Price, E. W.; Patrick, B. O.; Wester, D. W.; Adam, M. J.; Orvig, C. *J. Am. Chem. Soc.* **2010**, *132*, 15726−15733.
(16) Zhang, Y.; Hong, H.; Engle, J. W.; Bean, J.; Yang, Y.; Leigh, B. R.; Barnhart, T. E.; Cai, W. *PLoS One* **2011**, *6*, e28005.
(17) Bevilacqua, A.; Gelb, R. I.; Hebard, W. B.; Zompa, L. J. *Inorg. Chem.* **1987**, *26*, 2699−2706.
(18) Velikyan, I.; Maecke, H.; Langstrom, B. *Bioconjugate Chem.* **2008**, *19*, 569−573.
(19) Martell, A. E.; Motekaitis, R. J.; Clarke, E. T.; Delgado, R.; Sun, Y.; Ma, R. *Supramol. Chem.* **1996**, *6*, 353−363.
(20) Clarke, E. T.; Martell, A. E. *Inorg. Chim. Acta* **1991**, *181*, 273−280.
(21) Sun, Y.; Anderson, C. J.; Pajeau, T. S.; Reichert, D. E.; Hancock, R. D.; Motekaitis, R. J.; Martell, A. E.; Welch, M. J. *J. Med. Chem.* **1996**, *39*, 458−470.
(22) Liu, S.; Edwards, D. S. *Bioconjugate Chem.* **2000**, *12*, 7−34.
(23) Wu, C.; Kobayashi, H.; Sun, B.; Yoo, T. M.; Paik, C. H.; Gansow, O. A.; Carrasquillo, J. A.; Pastan, I.; Brechbiel, M. W. *Bioorg. Med. Chem.* **1997**, *5*, 1925−1934.
(24) Camera, L.; Kinuya, S.; Garmestani, K.; Wu, C.; Brechbiel, M. W.; Pai, L. H.; McMurry, T. J.; Gansow, O. A.; Pastan, I.; Paik, C. H.; Carrasquillo, J. A. *J. Nucl. Med.* **1994**, *35*, 882−889.
(25) Boswell, C. A.; Sun, X.; Niu, W.; Weisman, G. R.; Wong, E. H.; Rheingold, A. L.; Anderson, C. J. *J. Med. Chem.* **2004**, *47*, 1465−1474.
(26) Dale, A. V.; Pandya, D. N.; Kim, J. Y.; Lee, H.; Ha, Y. S.; Bhatt, N.; Kim, J.; Seo, J. J.; Lee, W.; Kim, S.; Yoon, Y.-R.; An, G. I.; Yoo, J. *ACS Med. Chem. Lett.* **2013**, *4*, 927−931.
(27) Shannon, R. *Acta Crystallogr.* **1976**, *A32*, 751−767.
(28) Price, E. W.; Zeglis, B. M.; Cawthray, J. F.; Ramogida, C. F.; Ramos, N.; Lewis, J. S.; Adam, M. J.; Orvig, C. *J. Am. Chem. Soc.* **2013**, *135*, 12707−12721.
(29) Holland, J. P.; Divilov, V.; Bander, N. H.; Smith-Jones, P. M.; Larson, S. M.; Lewis, J. S. *J. Nucl. Med.* **2010**, *51*, 1293−1300.
(30) Holland, J. P.; Williamson, M. J.; Lewis, J. S. *Mol. Imaging* **2010**, *9*, 1−20.
(31) Boros, E.; Ferreira, C. L.; Yapp, D. T. T.; Gill, R. K.; Price, E. W.; Adam, M. J.; Orvig, C. *Nucl. Med. Biol.* **2012**, *39*, 785−794.
(32) Boros, E.; Cawthray, J. F.; Ferreira, C. L.; Patrick, B. O.; Adam, M. J.; Orvig, C. *Inorg. Chem.* **2012**, *51*, 6279−6284.
(33) Boros, E.; Lin, Y.-H. S.; Ferreira, C. L.; Patrick, B. O.; Hafeli, U. O.; Adam, M. J.; Orvig, C. *Dalton Trans.* **2011**, *40*, 6253−6259.
(34) Boros, E.; Ferreira, C. L.; Patrick, B. O.; Adam, M. J.; Orvig, C. *Nucl. Med. Biol.* **2011**, *38*, 1165−1174.
(35) Bailey, G. A.; Price, E. W.; Zeglis, B. M.; Ferreira, C. L.; Boros, E.; Lacasse, M. J.; Patrick, B. O.; Lewis, J. S.; Adam, M. J.; Orvig, C. *Inorg. Chem.* **2012**, *51*, 12575−12589.
(36) Platas-Iglesias, C.; Mato-Iglesias, M.; Djanashvili, K.; Muller, R. N.; Elst, L. V.; Peters, J. A.; de Blas, A.; Rodríguez-Blas, T. *Chem.—Eur. J.* **2004**, *10*, 3579−3590.
(37) Ferreiros-Martinez, R.; Esteban-Gomez, D.; Platas-Iglesias, C.; Blas, A. d.; Rodríguez-Blas, T. *Dalton Trans.* **2008**, 5754−5765.
(38) Subramanian, R.; Colony, J.; Shaban, S.; Sidrak, H.; Haspel, M. V.; Pomato, N.; Hanna, M. G.; McCabe, R. P. *Bioconjugate Chem.* **1992**, *3*, 248−255.
(39) Frisch, M. J.; Trucks, G. W.; Schlegel, H. B.; Scuseria, G. E.; Robb, M. A.; Cheeseman, J. R.; Scalmani, G.; Barone, V.; Mennucci, B.; Petersson, G. A.; Nakatsuji, H.; Caricato, M.; Li, X.; Hratchian, H. P.; Izmaylov, A. F.; Bloino, J.; Zheng, G.; Sonnenberg, J. L.; Hada, M.; Ehara, M.; Toyota, K.; Fukuda, R.; Hasegawa, J.; Ishida, M.; Nakajima, T.; Honda, Y.; Kitao, O.; Nakai, H.; Vreven, T.; Montgomery, J. A., Jr.; Peralta, J. E.; Ogliaro, F.; Bearpark, M.; Heyd, J. J.; Brothers, E.; Kudin, K. N.; Staroverov, V. N.; Kobayashi, R.; Normand, J.; Raghavachari, K.; Rendell, A.; Burant, J. C.; Iyengar, S. S.; Tomasi, J.; Cossi, M.; Rega, N.; Millam, J. M.; Klene, M.; Knox, J. E.; Cross, J. B.; Bakken, V.; Adamo, C.; Jaramillo, J.; Gomperts, R.; Stratmann, R. E.; Yazyev, O.; Austin, A. J.; Cammi, R.; Pomelli, C.; Ochterski, J. W.; Martin, R. L.; Morokuma, K.; Zakrzewski, V. G.; Voth, G. A.; Salvador, P.; Dannenberg, J. J.; Dapprich, S.; Daniels, A. D.; Farkas, O.; Foresman, J. B.; Ortiz, J. V.; Cioslowski, J.; Fox, D. J. *Gaussian 09*, revision C.01; Gaussian, Inc.: Wallingford, CT, 2009.
(40) Dolg, M.; Stoll, H.; Preuss, H. *J. Chem. Phys.* **1989**, *90*, 1730−1734.
(41) Dolg, M.; Wedig, U.; Stoll, H.; Preuss, H. *J. Chem. Phys.* **1987**, *86*, 866−872.
(42) Price, E. W.; Cawthray, J. F.; Adam, M. J.; Orvig, C. *Dalton Trans.* **2014**, *43*, 7176−7190.
(43) Gran, G. *Analyst* **1952**, *77*, 661−671.
(44) Duckworth, P. Private communication.
(45) Gans, P.; Sabatini, A.; Vacca, A. *Talanta* **1996**, *43*, 1739−1753.
(46) Baes, C. F., Jr.; Mesmer, R. E. *The Hydrolysis of Cations*; Wiley-Interscience: New York, 1976.
(47) Brechbiel, M. W.; Gansow, O. A.; Atcher, R. W.; Schlom, J.; Esteban, J.; Simpson, D.; Colcher, D. *Inorg. Chem.* **1986**, *25*, 2772−2781.
(48) Price, E. W.; Zeglis, B. M.; Lewis, J. S.; Adam, M. J.; Orvig, C. *Dalton Trans.* **2014**, *43*, 119−131.
(49) Masuda, R.; Oishi, S.; Ohno, H.; Kimura, H.; Saji, H.; Fujii, N. *Bioorg. Med. Chem.* **2011**, *19*, 3216−3220.
(50) Dioury, F.; Guéné, E.; Scala-Roulleau, A. D.; Ferroud, C.; Guy, A.; Port, M. *Tetrahedron Lett.* **2005**, *46*, 611−613.
(51) Favre-Réguillon, A.; Segat-Dioury, F.; Nait-Bouda, L.; Cosma, C.; Siaugue, J.-M.; Foos, J.; Guy, A. *Synlett* **2000**, *2000*, 0868−0871.
(52) Fukuyama, T.; Jow, C.-K.; Cheung, M. *Tetrahedron Lett.* **1995**, *36*, 6373−6374.
(53) Salvatore, R. N.; Yoon, C. H.; Jung, K. W. *Tetrahedron* **2001**, *57*, 7785−7811.
(54) Stimmel, J. B.; Stockstill, M. E.; Kull, F. C. *Bioconjugate Chem.* **1995**, *6*, 219−225.
(55) Blower, P. J.; Lewis, J. S.; Zweit, J. *Nucl. Med. Biol.* **1996**, *23*, 957−980.
(56) Liu, S.; He, Z.; Hsieh, W.-Y.; Fanwick, P. E. *Inorg. Chem.* **2003**, *42*, 8831−8837.
(57) Liu, S.; Pietryka, J.; Ellars, C. E.; Edwards, D. S. *Bioconjugate Chem.* **2002**, *13*, 902−913.
(58) Tóth, É.; Brücher, E. *Inorg. Chim. Acta* **1994**, *221*, 165−167.
(59) Cacheris, W. P.; Nickle, S. K.; Sherry, A. D. *Inorg. Chem.* **1987**, *26*, 958−960.
(60) Loncin, M. F.; Desreux, J. F.; Merciny, E. *Inorg. Chem.* **1986**, *25*, 2646−2648.
(61) Clarke, E. T.; Martell, A. E. *Inorg. Chim. Acta* **1991**, *190*, 37−46.
(62) Harris, W. R.; Pecoraro, V. L. *Biochemistry* **1983**, *22*, 292−299.
(63) Raymond, K. N.; Müller, G.; Matzanke, B. *Top. Curr. Chem.* **1984**, *123*, 49−102.
(64) Kappel, M. J.; Raymond, K. N. *Inorg. Chem.* **1982**, *21*, 3437−3442.
(65) Geraldes, C. F. G. C.; Delgado, R.; Urbano, A. M.; Costa, J.; Jasanada, F.; Nepveu, F. *J. Chem. Soc., Dalton Trans.* **1995**, 327−335.

(66) Martell, A. E.; Smith, R. M. *Critical Stability Constants*; Plenum Press: New York, 1974−1989; Vol. *1*−*6*.
(67) Harris, W. R.; Chen, Y.; Wein, K. *Inorg. Chem.* **1994**, *33*, 4991−4998.
(68) Harris, W. R.; Yang, B.; Abdollahi, S.; Hamada, Y. *J. Inorg. Biochem.* **1999**, *76*, 231−242.
(69) Cooper, M. S.; Ma, M. T.; Sunassee, K.; Shaw, K. P.; Williams, J. D.; Paul, R. L.; Donnelly, P. S.; Blower, P. J. *Bioconjugate Chem.* **2012**, *23*, 1029−1039.